JGR Earth Surface

RESEARCH ARTICLE
10.1029/2024JF008058

Systematic Slowing of Initially Rapid Retreat of New Coasts Formed by Historical Eruptions in Volcanic Islands

Zhongwei Zhao[1], Neil C. Mitchell[2], Rui Quartau[3,4], and Ricardo S. Ramalho[5]

[1]South China Sea Institute of Oceanology, Chinese Academy of Sciences, Guangzhou, China, [2]Department of Earth and Environmental Sciences, University of Manchester, Manchester, UK, [3]Divisão de Geologia Marinha, Instituto Hidrográfico, Lisboa, Portugal, [4]Faculdade de Ciências, Instituto Dom Luiz, Universidade de Lisboa, Lisboa, Portugal, [5]School of Earth and Environmental Sciences, Cardiff University, Cardiff, UK

Abstract Due to their exposure to waves, volcanic island coasts typically retreat with cliff collapses and other erosional processes. Understanding how retreat rates vary over time and in response to environmental and other factors could be useful for geohazard assessment, coastal management and landform reconstruction. Historical eruptions can create new coasts with volcanic materials that are friable. The retreat of such coastlines can be fast and more easily observed than for many older rocky coasts. Here we assemble coastline retreat distances and rates of 12 coasts formed by historical eruptions from literature sources and remote-sensing data. In the cases with observations at many time steps, post-eruptive coastline retreat was initially rapid and declined with time. We adapt an empirical equation found earlier to represent the coastline retreat of a Surtseyan cone, finding that it represents the systematic variation in retreat distances with time well where coastal evolution is known in more than 5 time steps. The slowing is interpreted to arise from (a) increasing wave attenuation with abrasion platform widening, (b) exposure of progressively more resistant materials at cliffs, and (c) from increasingly taller cliffs, which lead to increasingly large volumes of debris from cliff collapses, temporarily protecting cliff bases. Coastline retreat rates also follow inverse power-law relationships with varied time intervals of measurement; hence, they are affected by erosion episodicity. Comparisons with wave height and precipitation surprisingly reveal no strong co-variation with the retreat rates. We hypothesize that varied lithology, fracture density and other factors dominate retreat rates of young volcanic coastlines.

Plain Language Summary When volcanic eruptions create new land, they form new coasts exposed to waves that can collapse abruptly. These coasts often consist of friable material, making them easily eroded by waves. We studied coastline changes at 12 coasts formed by historical volcanic eruptions. In the cases with observations at multiple stages, the coast retreated rapidly shortly after the eruptions, but then retreated more gradually. How they retreated with time can be well represented by an equation found earlier for a coastal volcano in the Azores, Portugal. We attribute the slowing of erosion primarily to wave energy loss on widened submarine platforms. Slowing is also potentially due to erosion, removing friable material and exposing harder, more resistant rocks. Furthermore, volcanic coasts often have steep, rising terrain landward, so when cliffs collapse, they generate larger piles of debris that further protect the cliffs. Surprisingly, erosion rates did not vary with the size of local waves or rainfall. Instead, local rock type and fracture density may dominate how quickly these young volcanic coasts erode.

Key Points:

- Retreat rates of coastlines formed by historical volcanic eruptions slowed systematically over time
- No systematic covariation of retreat rates with wave height or precipitation was found
- Retreat distances approximated by an inverse power law function of time

Supporting Information:

Supporting Information may be found in the online version of this article.

Correspondence to:

N. C. Mitchell,
neil.mitchell@manchester.ac.uk

Citation:

Zhao, Z., Mitchell, N. C., Quartau, R., & Ramalho, R. S. (2025). Systematic slowing of initially rapid retreat of new coasts formed by historical eruptions in volcanic islands. *Journal of Geophysical Research: Earth Surface*, *130*, e2024JF008058. https://doi.org/10.1029/2024JF008058

Received 5 OCT 2024
Accepted 16 AUG 2025

Author Contributions:

Conceptualization: Zhongwei Zhao, Neil C. Mitchell
Data curation: Zhongwei Zhao
Formal analysis: Zhongwei Zhao, Neil C. Mitchell
Funding acquisition: Zhongwei Zhao, Rui Quartau
Investigation: Zhongwei Zhao, Neil C. Mitchell
Resources: Neil C. Mitchell, Rui Quartau, Ricardo S. Ramalho
Supervision: Neil C. Mitchell, Rui Quartau
Writing – original draft: Zhongwei Zhao
Writing – review & editing: Neil C. Mitchell, Rui Quartau, Ricardo S. Ramalho

1. Introduction

Volcanic eruptions can create new land (Lasky, 2012; Simkin et al., 2000) by emplacing lava deltas (Lipman & Moore, 1996; Rodriguez-Gonzalez et al., 2022). Surtseyan-style eruptions in shallow marine locations can also form new land by building submarine pyroclastic mounds crowned by emergent tuff cones (Machado et al., 1962; Romagnoli & Jakobsson, 2015; Xu et al., 2015). For example, the Surtseyan cone at Capelinhos comprises the following five facies (Cole et al., 2001). At its base, Facies I contains evenly thick tephra fallout beds. It is overlain in sequence upwards with: Facies II, undulating beds of pyroclastic surge deposits; Facies III, evenly thick bed of simultaneous tephra fallout and pyroclastic surge deposits; Facies IV, alternating beds of coarse aggregates and fine ash; and Facies V, thin scoria lapilli deposits from Hawaiian-style explosions. The facies sequence is generally similar in other Surtseyan cones (Sorrentino et al., 2011). Subaerial lava flows were also emplaced at later eruption stages at Capelinhos and Surtsey, when the vents of these volcanoes were isolated from

sea water and the eruption-style transitioned from hydromagmatic (Surtseyan and/or Taalian) to magmatic (Hawaiian and/or Strombolian) (Jakobsson, 1972; Machado et al., 1959).

Once eruptions cease, coasts are eroded by waves, wind and precipitation, eventually involving cliff failure (Ramalho et al., 2013). Consequently, coastlines can change rapidly (Ferrer-Valero et al., 2019; Norrman, 1985; Romagnoli et al., 2006). For example, the Capelinhos coasts retreated ∼164 m on average in the first six months after the eruption (Zhao et al., 2019). Many volcanic island coasts are densely populated and newly formed land is often adopted for agriculture and other purposes. For instance, the 2021 La Palma lava flows crossed a coastal plain of older lava that had been adopted for agriculture (Román et al., 2022). Better prediction of future coastal changes would be useful for planning coastal infrastructure, assessing risks and making insurance decisions. In addition, these coasts are also potentially useful for geological education (Németh & Gravis, 2022; Németh & Moufti, 2023), and some have been listed as World Heritage sites (e.g., Surtsey) and Global Geopark (e.g., Capelinhos) by UNESCO (Ávila et al., 2023; Németh et al., 2006; Roman, 2023). Furthermore, erosion rates provide key insights into the risks associated with cliff failures (Ávila et al., 2023; Jakob & Lambert, 2009).

In general, rocky coasts retreat slowly so changes are difficult to monitor, and the evidence of past erosion events (e.g., cliff failures and their associated debris) is rapidly removed by wave action (Hall et al., 2008). Moreover, erosion of rocky coastlines is typically threshold-driven and progresses intermittently rather than at constant rates. Changes occur when wave force exceeds the strength threshold of cliff rocks and when gravitational instability leads to mechanical failure (Naylor & Stephenson, 2010; Phillips, 2006; Ramalho et al., 2013; Sunamura, 1977). Consequently, our ability to predict their erosion is limited (Moses & Robinson, 2011; Prémaillon et al., 2018).

In contrast, the coastlines of newly formed and young volcanic islands commonly comprise friable pyroclastic materials or their immediately reworked equivalents. Consequently, they are more vulnerable to wave erosion and coastline changes can be fast and more easily recorded in historical surveys or, for recent events, in remote-sensing data. In this early stage, rates tend to decrease over time (Mogi et al., 1980; Richards, 1961; Romagnoli et al., 2006; Xu et al., 2015; Zhao et al., 2019). This slowing of rates aligns with some numerical simulations of widening of platforms by rock cliff retreat, which tend to be rapid initially but more slowly later as a result of wave attenuation (Trenhaile, 2000). Wave type also influences the wave assailing force on cliffs (Matsumoto et al., 2024; Sunamura, 1995). Waves will have less force if they break before reaching the cliffs than if they break at cliff bases. Hence, as waves lose energy while traveling across platforms, erosion rates may not have a simple or direct relationship with platform width.

In this study, coastline changes of 12 widely distributed coasts formed by volcanic eruptions were compiled, allowing us to investigate how they vary with the elapsed time since eruption. Environmental factors such as wave power (proportional to the square of wave height) and precipitation are also suspected to affect retreat rates (Huppert et al., 2020; Jones et al., 2015; Trenhaile, 2014, 2019; Young et al., 2009, 2021). Using modern wave and precipitation data from the fifth generation European Center for Medium range Weather Forecasts (ECMWF) reanalysis (ERA5), we assess whether long-term coastal retreat rates vary systematically with these parameters. We further discuss the implications of the results for coastal management, hazard evaluation and morphological evolution.

2. Background

2.1. Description of Volcanic Eruptions and Environment

The 12 volcanic coasts in this study are distributed widely (Figure 1a): four in the Atlantic Ocean (Heimaey, Surtsey, Capelinhos and La Palma), four in the Pacific Ocean (Kasatochi, Nishinoshima Shinto, Barcena and Hunga Tonga Hunga Ha'apai), two in the southern Red Sea (Sholan and Jadid), one between the Pacific and Indian oceans (Anak Krakatau) and one near Antarctica (Deception). They were formed from 1952 to 2021 (Table 1) by eruptions that lasted from a single day (Kasatochi and Deception) to over four years (Surtsey). In this study, coasts were lithologically classified simply into lava flow, tephra, or mixed coasts based on visual interpretation of published resources (Table 2). Most coasts (6/12) consist of tephra, while one-fourth are composed of lava flows. The three coasts comprise both lava flows and tephra (termed “mixed” here).

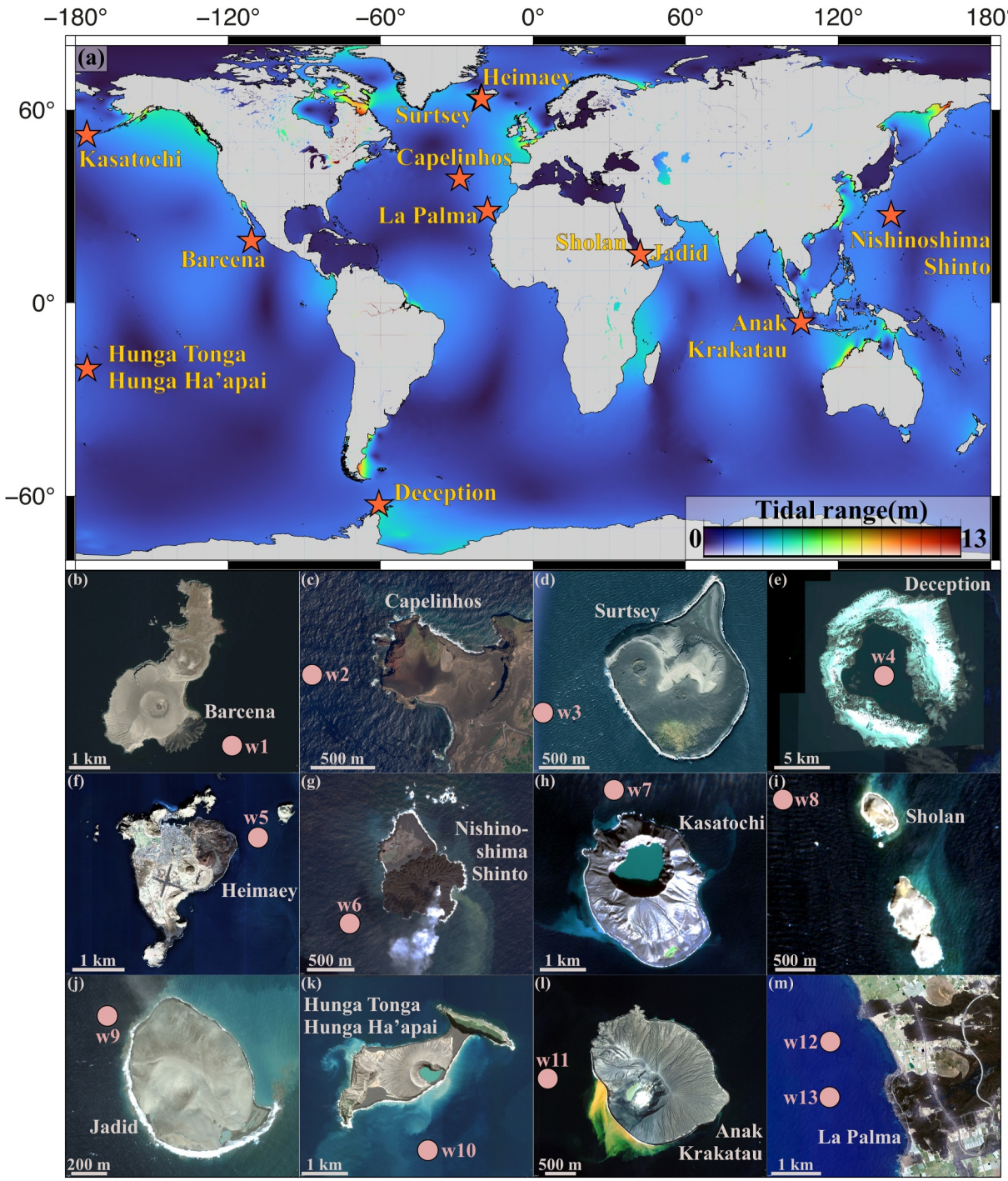

Figure 1. (a) Locations of volcanic coasts formed by historical eruptions studied here. Background colors represent tidal ranges from the Finite Element Solution 2014 tidal model. (b–m) Google Earth™ Images (freely available for non-commercial/academic use under the terms and conditions of the Google Earth/Maps Terms of Service). Pink circles and w1–w13 locate where wave and precipitation data were extracted from ERA5 outputs.

2.1.1. Barcena, 1952–53 (19.31°N, 110.80°W)

Volcano Barcena (Figure 1b) is a tuff cone at the southern end of Isla San Benedicto, Mexico, ~350 km off the SE coast of the Baja California peninsula (Richards, 1965). The Barcena eruption started on 1 August 1952 and formed a tuff cone by the next day (Richards & Brattstrom, 1959). A lava delta was extruded on the SE side of the cone from 8 December 1952 to 27 February 1953, advancing the earlier coastline ~800 m seaward

Journal of Geophysical Research: Earth Surface

10.1029/2024JF008058

Table 1
Compilation of Changes in Coasts Formed by Historical Eruptions From Existing Studies

ID	Source	Location	Eruption-style	Type of resulting volcanic edifice	Type of eroded coast analyzed here	Tidal range (m)[a]	Dates of eruption	Measuring intervals	Coastline type described in sources	Coastline survey method	Rates used in this study[b]
1	Richards (1965)	Volcano Barcena, California	Surtseyan and effusive	Tuff cone and lava delta	Volcanic edifice and lava delta	2.65	1 August 1952–27 February 1953	a) April–September 1953	a) Lava flow	Aerial photos (Aerial photogrammetric surveys)	1
								b) August–December 1952	b) Unconsolidated tephra		1
2	Machado et al. (1962), Zhao et al. (2019)	Capelinhos, Azores	Surtseyan and Strombolian	Overlapping tuff and scoria cone, and lava shield/delta	Volcanic edifice	1.30	27 September 1957–4 November 1958	November 1958–October 2014	Lava flow and unconsolidated tephra	1958–1981, historical maps (Field surveys)	1
										2004–2014, satellite images (Google Earth)	
3	Romagnoli et al. (2006)	Surtsey, Iceland	Surtseyan and Strombolian	Overlapping tuff and scoria cone, and lava shield/delta	Volcanic edifice	8.08	8 November 1963–5 June 1967	a) August 1964–July 2006	a) Unconsolidated tephra and tuff	Aerial photos (Aerial photogrammetric surveys)	1
								b) July 1967–July 2012	b) Lava flow		1
4	Torrecillas et al. (2024)	Deception Island, Antarctic	Taalian	Tuff rings	Volcanic edifice	1.49	12–13 August 1970	December 1970–February 2020	Unconsolidated tephra	1970, historical map (Aerial Orthophoto)	1
										2003–2020, satellite images (QuickBird, KOMPSAT-3 and Sentinel-2)	
5	Eiríksson (1990)	Heimaey, Iceland	Strombolian	Scoria cone and lava delta	Lava delta	8.13	23 January 1973–3 July 1973	1973–1990	Lava flow	Aerial photos (Aerial photogrammetric surveys)	2
6	Mogi et al. (1980)	Nishinoshima Shinto, Japan	Surtseyan and Strombolian	Overlapping tuff and cinder cones, and lava shield/delta	Volcanic edifice	0.48	12 April 1973–10 June 1974	August 1974–August 1976	Lava flow	Aerial photos (Aerial photogrammetric surveys)	2
7	Waythomas, Scott and Nye (2010), Waythomas, Scott, Prejean, et al. (2010)	Kasatochi Volcano, Alaska	Phreatomagmatic (possibly Taalian)	Strato-volcano with pyroclastic fan deltas	Volcanic edifice and pyroclastic fan deltas	2.30	7–8 August 2008	August 2008–September 2009	Unconsolidated tephra	Satellite images (QuickBird)	1

Journal of Geophysical Research: Earth Surface

10.1029/2024JF008058

Table 1
Continued

ID	Source	Location	Eruption-style	Type of resulting volcanic edifice	Type of eroded coast analyzed here	Tidal range (m)[a]	Dates of eruption	Measuring intervals	Coastline type described in sources	Coastline survey method	Rates used in this study[b]
8	Xu et al. (2015)	Sholan, Red Sea	Surtseyan	Tuff cone	Volcano edifice	1.73	13 December 2011–12 January 2012	January 2012–July 2017	Unconsolidated tephra	Satellite images (WorldView-2)	1
9	Xu et al. (2015)	Jadid, Red Sea	Surtseyan	Tuff cone	Volcano edifice	1.73	28 September 2013–20 November 2013	November 2013–February 2014	Unconsolidated tephra	Satellite images (WorldView-2)	1
10	Garvin et al. (2018)	Hunga Tonga Hunga Ha'apai	Surtseyan	Tuff cone	Volcanic edifice	1.31	19 December 2014–26 January 2015	January 2015–September 2017	Unconsolidated tephra and tuff	Satellite images (WorldView and Pleiades)	2
11	Novellino et al. (2020)	Anak Krakatau, Indonesia	Surtseyan and Taalian	Tuff cone/ring	Volcanic edifice	3.29	21 June 2018–1 November 2019	May–November 2019	Unconsolidated tephra	Satellite images (Sentinel-2)	2
12	Hutton (2023)	La Palma, Canary	Strombolian	Scoria cone and lava shield/ deltas	Lava delta	0.80	19 September 2021–13 December 2021	December 2021–February 2023	Lava flow	Satellite images (Pleiades)	1

[a]Tidal range estimated from the FES2014 (Finite Element Solution 2014) tidal model. [b]Rates taken from (1) published sources and (2) measurements in this study from coastlines interpreted from the images.

Table 2
Summary of the Highest Average Coastline Retreat Rates (HACR) Reported at Each Locality of Volcanic Coasts Along With Properties From ERA5

Sites and coast ID	Coastline type and sections classified in this study	HACR (m/yr)	Time interval (days)	Mean elapsed time since last eruption (days)	Maximum wave height when erosion was the fastest (m)	Maximum monthly precipitation (m/month)[a]
Barcena 1	Lava	122.28	34	65	2.64	0.03
Barcena 2	Tephra	620.50	121	69.5	3.85	6.08
Capelinhos 1	Tephra, north	56.00	178	92	3.12	0.00
Capelinhos 2	Tephra, south	188.00	181	92	3.12	0.00
Capelinhos 3	Mixed, north	326.00	181	92	3.12	0.00
Capelinhos 4	Mixed, south	62.00	181	92	3.12	0.00
Capelinhos 5	Lava, north	150.00	181	92	3.12	0.00
Capelinhos 6	Lava, south	199.00	181	92	3.12	0.00
Capelinhos 7	Mixed, all sectors	164.00	181	92	3.12	0.00
Surtsey 1	Tephra	30.00	1,064	799	11.97	3.75
Surtsey 2	Lava	107.50	366	1,514	9.54	3.01
Deception	Tephra	6.50	11,719	5,969.5	7.60	2.54
Heimaey	Lava	1.29	6,271	3,135.5	14.49	4.56
Nishinoshima Shinto	Lava	49.14	87	268.5	8.20	4.50
Kasatochi 1	Tephra, NW	328.50	40	20	2.99	3.62
Kasatochi 2	Tephra, NE	321.20	40	20	2.99	3.62
Kasatochi 3	Tephra, SE	448.95	40	20	2.99	3.62
Kasatochi 4	Tephra, SW	324.85	40	20	2.99	3.62
Kasatochi 5	Tephra, average	355.88	40	20	2.99	3.62
Sholan	Tephra	15.00	2023	1,013.5	3.42	5.82
Jadid	Tephra	26.00	85	42.5	2.98	0.83
Hunga Tonga Hunga Ha'apai	Tephra	94.57	33	16.5	2.31	3.21
Anak Krakatau	Tephra	129.61	10	491	1.71	0.06
La Palma 1	Lava, north rock promontories	711.75	1	38.5	2.04	0.00
La Palma 2	Lava, north whole	584.79	1	37.5	2.05	0.00
La Palma 3	Lava, south rock promontories	434.35	1	221.5	1.58	0.00
La Palma 4	Lava, south whole	155.40	10	168	2.39	0.09

[a]0.00 indicates that actual values of ERA5 are less than 0.005 m/month.

(Brattstrom, 2015). A volume of ~3,200 m^2 of new lava flows and unconsolidated tephra was estimated when the eruption stopped in February 1953 (Richards, 1966). Richards (1965) reported a retreat rate of 1.7 m/day for tephra cliffs in the fall of 1952 based on time-lapse aerial photos. Nearly 0.71×10^6 m^3 of unconsolidated tephra were eroded by waves within just 40 days of their emplacement (Richards, 1965). Six months of observations in 1953 revealed a retreat rate of 0.12 m/day for a lava deltas (Richards, 1961). Prevailing waves and swells affecting Isla San Benedicto are from the north, with occasional storm waves from the SE during hurricane seasons (July–October) (Richards, 1965). The annual precipitation is less than ~150 mm at the island, which has a warm and arid climate (Putnam et al., 1960; Richards, 1961).

2.1.2. Capelinhos, 1957–58 (38.60°N, 28.83°W)

Capelinhos volcano (Figure 1c) sits on the western-most tip of Faial Island in the Azores Archipelago (Madeira et al., 2015). The eruption started underwater on 27 September 1957 and ceased in November 1958. During its

duration, the eruption first created a tuff cone through Surtseyan and briefly Taalian activity, subsequently transitioning to a Strombolian-style when the vent was fully isolated from sea water. A cinder cone was formed inside the tuff cone, allowing for the extrusion of a small lava shield/delta from the base of the cone (Machado et al., 1962). New land of ~2.5 km^2 area and ~0.15 km^3 volume was created, which consisted of lava flows (56% by volume) and unconsolidated tephra (44%) (Machado et al., 1962; Madeira, 2007). This area decreased to ~0.67 km^2 by 2007 (Forjaz, 2007) and to ~0.42 km^2 by 2014 (Zhao et al., 2019). Erosion rates of its coasts averaged ~164 m/yr in May 1959, declining to ~1–3 m/yr by October 2014 and varying strongly between a lava flow and tephra cliffs (Zhao et al., 2019). The preceding swells mainly originate from NW (29%) and W (24%). Capelinhos is exposed to waves generated during violent hurricanes, which occur every 7 years on average (Andrade et al., 2008) with significant wave heights exceeding 16 m (Carvalho, 2003). The Azores oceanic temperate climate is controlled by seasonal anticyclones, which contribute 75% of the islands' total annual precipitation of ~600 mm/yr at sea level (Forjaz, 2004).

2.1.3. Surtsey, 1963–67 (63.30°N, 20.60°W)

Surtsey (Figure 1d) lies ~30 km off the south coast of Iceland (Claudino-Sales, 2019). The eruption commenced underwater on 8 November 1963 and lasted ~4 years until the last observed lava flows on 5 June 1967 (Romagnoli & Jakobsson, 2015; Thorarinsson & Eysteinsson, 1967). Like Capelinhos, the eruption first created a tuff cone through Surtseyan activity, subsequently transitioning to a Strombolian style. The eruption produced a km^3 volume of tephra (70%) and lava flows (30%) (Thorarinsson, 1969). Its total land area in June 1967 was ~2.65 km^2 and reduced to ~1.31 km^2 by July 2012 (Romagnoli & Jakobsson, 2015). Rates of cliff retreat of the south and southwest a lava flow coasts were 20–35 m/yr between 1969 and 1970 (Norrman, 1972), and decreased to ~11–12 m/yr over the subsequent 45 years (Norrman, 1978; Romagnoli & Jakobsson, 2015). The tephra coasts retreated by ~30 m/yr during the eruption (1964–1967) but progressively declined to ~0.2–0.3 m/yr by 2006 (Jakobsson et al., 2000; Norrman, 1985; Romagnoli & Jakobsson, 2015). Erosion of the Surtsey coasts left a nearly horizontal submarine platform (Sunamura, 2021). Surtsey is exposed to frequent and powerful storms in the North Atlantic Ocean (Etienne & Paris, 2010), with significant wave heights reaching 16 m (Viggósson & Grétarsson, 2010). Prevailing waves (~52% of time) are mainly from W and SW (Norrman & Erlingsson, 1992). Surtsey has a mild but windy subpolar oceanic climate with a maximum annual precipitation of 1071.8 mm (Petersen & Jónsson, 2020).

2.1.4. Deception, 1970 (62.96°S, 60.62°W)

Deception Island (Figure 1e) hosting a caldera volcano is located in the South Shetland Islands within the Bransfield Strait, ~120 km north of the Antarctic Peninsula (Geyer et al., 2021). Deception has erupted more than 20 times in the past two centuries, with the most recent one between 12 August 1970 and 13 August 1970 (Smellie et al., 2002). The 1970 eruption, which occurred at Telefon Bay on the northern shore of the flooded caldera (Port Foster), involved over 13 vents both onshore and offshore (but nearshore), all of which were characterized by phreatomagmatic activity, dominantly Taalian in-style (Pedrazzi et al., 2014). The eruption produced ~0.10 km^3 of unconsolidated tephra (Torrecillas et al., 2012). The land area reduced in 1970–2003 by 0.007 km^2/yr and decreased more slowly in 2003–2020 by 0.002 km^2/yr (Torrecillas et al., 2024). Waves affect the island mainly from the NW and NE. It is also influenced by energetic waves (wave heights >10 m) propagating from the Drake Strait into the Bransfield Strait (Lonin et al., 2022). However, the tephra coast is mainly within the northern shore of Port Foster and is sheltered from the most energetic waves by the narrow Neptunes Bellows (Angulo-Preckler et al., 2021). Deception has a polar maritime climate and annual precipitation (snow and rain) of ~500 mm (Smith et al., 2003).

2.1.5. Heimaey, 1973 (63.44°N, 20.23°W)

Heimaey (Figure 1f) lies ~7 km off the south coast of Iceland (Mattsson & Höskuldsson, 2003). In January 1973, the Eldfell eruption started on the east side of the island. It was Strombolian/Hawaiian and led to the extrusion of an a lava flow field (Morgan, 2000). The eruption ceased in early July 1973 (Williams & Moore, 1983) after forming a ~2.2 km^2 ‘a‘ā lava delta on the SE end of the island (Eiríksson, 1990). Coastal positions in 1973 and 1990 have been reported (Eiríksson, 1990). The island faces frequent waves from W and SW with heights of 16 m (Viðarsdóttir, 2019). Heimaey has a windy subpolar oceanic climate with its maximum annual precipitation exceeding 1,000 mm (Hansom et al., 2014; Morgan, 2000).

2.1.6. Nishinoshima Shinto, 1973–74 (27.25°N, 140.88°E)

The Nishinoshima Shinto (NS) Island (Figure 1g) is part of the Ogasawara island arc, ∼1,000 km south of Tokyo, Japan (Baba et al., 2020). The island is the subaerial tip of a much larger submarine volcano. In early April 1973, a Surtseyan eruption formed the island, eventually transitioning to Strombolian and leading to the formation of a lava shield/delta, with ∼0.017 km^3 of lava flows (pahoehoe), which completely covered the deposits of the Surtseyan phase. Approximately 0.316 km^2 of land had formed when the eruption finished in summer 1974 (Kudo & Hoshizumi, 2006). Two stages of rapid coastline change were observed between 1974 and 1976. Coastlines retreated more than 120 m between August and October 1974, and 50 m from November 1975 to August 1976 (Mogi et al., 1980). No independent characterization of wave climate and precipitation appears available for NS, but waves are mainly from E and SE in the NW Pacific Ocean (Li et al., 2023). The region has a subtropical climate with a mean annual precipitation of 1,277 mm (1971–2000) (Claudino-Sales, 2019).

2.1.7. Kasatochi, 2008 (52.17°N, 175.51°W)

Kasatochi Island (Figure 1h) is a strato-volcano located within the west-central Aleutian Islands of Alaska, USA (Scott et al., 2010). An explosion on 7 August 2008 marked the beginning of the eruption, which lasted 24 hr in five phases and ceased on 8 August 2008 (Waythomas, Scott, & Nye, 2010). Nearly 0.15–0.28 km^3 of unconsolidated tephra were produced by the eruption, extending the previous coastline by ∼400 m in places, mostly where pyroclastic fan deltas were formed from pyroclastic density currents (Waythomas, Scott, Prejean, et al., 2010). Coastline erosion rates were estimated to be 0.22–0.39 m/day from 8 August 2008 to 13 September 2009 (Waythomas, Scott, & Nye, 2010). Kasatochi Island is influenced by storm-generated waves traveling from west to east, especially during winter (Rodionov et al., 2005). Kasatochi has a windy and wet maritime climate, with a maximum hourly rainfall of 5.1 mm (Waythomas, Scott, & Nye, 2010).

2.1.8. Sholan, 2011–12 (15.14°N, 42.09°E) and Jadid, 2013 (15.10°N, 42.13°E)

Sholan (Figure 1i) and Jadid (Figure 1j) are volcanic islands in the southern Red Sea, lying ∼50 km off the coast of Yemen (Jónsson & Xu, 2015). Sholan initially formed from a submarine (Surtseyan) eruption on 13 December 2011 with a single vent. The eruption lasted 25 days and produced an unconsolidated tephra cone of ∼0.25 km^2 at the end of the eruption. It then lost 0.01 km^2 in the following 2 months and 30% after 2 years (Xu et al., 2015). Jadid also started forming underwater, emerging on 28 September 2013 and further south, through Surtseyan activity. The eruption continued for ∼54 days and built an unconsolidated tephra island (tuff cone) with an area of ∼0.68 km^2 (Jónsson & Xu, 2015). During the early stages after the eruption, the erosion of Jadid was less severe than that of Sholan. Its area had decreased only modestly to 0.67 km^2 by late February 2014 (Xu et al., 2015). Waves in Zubair vary in direction because of the seasonal reversal of monsoon winds from NE (summer) to SW (winter) (Sofianos & Johns, 2003). The climate is tropical to subtropical humid, with an average annual precipitation of only 60 mm (Hasanean & Almazroui, 2015).

2.1.9. Hunga Tonga Hunga Ha'apai, 2014–15 (20.55°S, 175.39°W)

Hunga Tonga Hunga Ha‘apai (HTHH, Figure 1k) was the southwestern-most member of the Ha'apai volcano group in the South Pacific Ocean, ∼65 km off the northern shore of the Tongan capital, Nuku‘alofa (Vaughan & Webley, 2010). HTHH was formed when a Surtseyan eruption, which started on the 19 December 2014, created a tuff cone that joined the islands of Hunga Tonga and Hunga Ha'apai, all located on the caldera rim of the larger submarine Hunga volcano (Brenna et al., 2022; Vaughan & Webley, 2010). By the end of the eruption in late January 2015, new land of ∼1.74 km^2 consisting of unconsolidated tephra had formed (Garvin et al., 2018), that is, a tuff cone. The volumetric erosion rate of HTHH was 0.0026 km^3/yr over a 36-month period, suspected primarily by waves (Garvin et al., 2018). HTHH was subsequently destroyed by the hydromagmatic explosion of 15 January 2022, with only two small islets left remaining from the original island (Clare et al., 2023; Omira, Ramalho, et al., 2022; Seabrook et al., 2023; Terry et al., 2022). HTHH was affected by waves originating from the dominant SE trade winds and swell generated by storms in the Southern Ocean (Aguirre et al., 2017). The HTHH climate is tropical, with abundant rainfall and average annual precipitation exceeding 1,600 mm (Terry, 2007).

2.1.10. Anak Krakatau, 2018–19 (6.10°S, 105.42°E)

Anak Krakatau (AK, Figure 1l) is a volcanic island located between the islands of Java and Sumatra in Sunda Strait, ∼155 km west of Jakarta (Williams, Rowley, & Garthwaite, 2019). Eruptive activity has continued periodically at AK, including a tsunami following the collapse of the cone toward the end of the eruption in 2018 (Abdurrachman et al., 2018). The 2018 eruption began on 21 June 2018 and added ∼3.03 km^2 of unconsolidated tephra, largely through Surtseyan and occasionally Taalian activity. A collapse occurred later (22 December 2018), which reduced its volume by 0.102 km^3 (Walter et al., 2019). Coastline retreat was greatest on the southwest coast, starting in April 2019 (Novellino et al., 2020). AK is subjected to long-period waves (swell) originating from the Indian Ocean, which propagate SW into the Sunda Strait (Deplus et al., 1995). AK has a tropical climate, with an annual precipitation of 2,500–3,000 mm (Fiantis et al., 2021).

2.1.11. La Palma, 2021 (28.61°N, 17.93°W)

La Palma (LP) Island (Figure 1m) lies in the NW end of the Canary Islands (Carracedo et al., 2022). A Strombolian eruption started on 19 September 2021 on the western slope of Cumbre Vieja volcano, lasting 85 days until 13 December 2021 (Del Fresno et al., 2023; González, 2022). Nearly 0.15 km^3 of mainly a lava flows were produced, forming two deltas of ∼0.47 km^2 total area (Ferrer et al., 2023; Romero et al., 2022). Beaches of volcanic particles formed in just a few weeks after the eruption, reflecting the rapid initial erosion (Alonso et al., 2023; Hutton, 2023). Waves in the Canaries originate from N and NNE (Gonçalves et al., 2020). LP has a subtropical-Mediterranean climate with an average annual precipitation of ∼650 mm (Pérez et al., 2020).

3. Materials and Methods

3.1. A Model for Accumulative Coastline Change Distance (ACD) Variation With Elapsed Time

Accumulative coastline change distance (ACD), or otherwise w here, is the total distance of change of a coastline measured perpendicular to the coastline since the eruption or shortly thereafter. A previous study of coastlines at Capelinhos (Zhao et al., 2019) found that the rate of change with time t, dw/dt, followed an inverse power-law relationship with total coastline change distance w (i.e., ACD):

$$\frac{dw}{dt} = E_0 w^{-\alpha} \tag{1}$$

where E_0 is the rate coefficient (day^{-1}) and α is a dimensionless constant decay coefficient.

This equation can be recast in terms of w as a function of time. Rearranging Equation 1 produces:

$$\frac{dw}{w^{-\alpha}} = E_0 dt \tag{2}$$

$$w^{\alpha} dw = E_0 dt \tag{3}$$

Equation 3 can be integrated:

$$\int_{w0}^{w1} w^{\alpha} dw = \int_{t0}^{t1} E_0 dt \tag{4}$$

$$\left| \frac{1}{\alpha + 1} w^{\alpha+1} \right|_{w0}^{w1} = |E_0 t + C|_{t0}^{t1} \tag{5}$$

When the elapsed time t is 0, $t_0 = 0$, $w_0 = 0$. Letting w_1 be simply w and t_1 be t (time elapsed since eruption), the evaluation leads to:

$$\frac{1}{\alpha + 1} w^{\alpha+1} = E_0 t \tag{6}$$

$$w^{\alpha+1} = (\alpha + 1) E_0 t \tag{7}$$

Thus, if a coast follows Equation 1, w should follow:

$$w = [(\alpha + 1) E_0 t]^{1/\alpha+1} \tag{8}$$

Therefore, this study aims to determine whether Equation 8 represents the varying coastline positions w of the 12 sites. Recent studies of coastal cliff evolution (e.g., Arróspide et al. (2023)), suggested that α is likely to have a constant value of 1 (equation derived in Supporting Information S1 of this article, Text S1 in Supporting Information S1). Thus, we conducted two tests when attempting to fit Equation 8 to the data. In Test 1, both α and E_0 were allowed to vary, while in Test 2 only E_0 was varied ($\alpha = 1$).

3.2. Coastline Change

Average coastline retreat rates (ACRs) of eight sites were taken from published values. They were originally measured from historical maps, aerial photos and/or satellite images, which have varied resolutions of 0.3–10 m (Table S1 in Supporting Information S1). The accuracy of coastline positions is affected by positional and measurement uncertainties (Fletcher et al., 2012), including errors from image resolution, rectification and shoreline digitization. Orthorectification errors are usually not straightforward to justify due to the lack of control points; therefore, they were only reported for Barcena, Capelinhos, Sholan, Hunga Tonga Hunga Ha'apai and La Palma. Digitizing error arises from difficulties in human interpretation of coastlines, limiting the best accuracy of pixel resolution (Romine et al., 2009). These errors can have significant impacts when retreats and measuring intervals are small (e.g., La Palma). Estimation of the least total positional errors is shown in Table S1 in Supporting Information S1. For Heimaey, Nishinoshima Shinto, Hunga Tonga Hunga Ha'apai (Figure S1 in Supporting Information S1) and Anak Krakatau (Figure S2 in Supporting Information S1), we digitized coastline positions from figures in the publications using ArcGIS 10.8. We then used the Digital Shoreline Analysis System (DSAS V5) module (https://www.usgs.gov/centers/whcmsc/science/digital-shoreline-analysis-system-dsas) to generate transects perpendicular to the coastline every 10 m along-coast, along which historical coastline positions were recorded. Cliff heights at Hunga Tonga Hunga Ha'apai were digitized from time-lapsed digital elevation models (from the supporting information of Garvin et al., 2018), along these transects using the "Samples" tool in ArcGIS. Changes in coastlines along those transects consequently represent the coastline change distance (CCD, with the mean shown in Figure 2). ACRs for each observation period and site were derived by dividing the CCD by the time interval between maps or satellite images. Both CCD and ACR are signed, with positive values denoting coastlines moving landward (erosion) and negative values indicating accretion. The ACR values averaged for each site are given in Table S2 in Supporting Information S1. We further obtained the ACD of each site by summing the distance increments i:

$$\mathrm{ACD} = \sum_{i=1}^{n} \mathrm{ACR}_i * t_i = \sum_{i=1}^{n} \mathrm{CCD}_i \tag{9}$$

Equation 8 was fitted in a least-squares sense to the variations in ACD with time, that is, equating ACD with w.

3.3. Environmental Conditions

Hourly significant wave height and total precipitation were extracted from ERA5 (https://www.ecmwf.int/en/research/climate-reanalysis) for sea positions adjacent to the sites marked in Figure 1b. Previous assessments of ERA reanalysis wave heights and precipitation have demonstrated the model's general accuracy, with a mean R^2 value of 0.8 when compared to wave height data from buoys and rain gauge observations (Bandhauer et al., 2022; Jiang et al., 2021; Rusu & Rusu, 2021). Our comparison of annual total precipitation derived from ERA5 with field rain gauge data from a site near Capelinhos (Coutinho, 2000) suggests an average underestimation of ~40% there (Figure S3 in Supporting Information S1).

At each site, we recorded maximum wave height (MWH) from the significant wave heights of waves propagating coastwards during each time interval between coastline observations. Similarly, maximum monthly total precipitation (MTP) was recorded from the precipitation values. Prevailing precipitation is mainly rainfall, except for

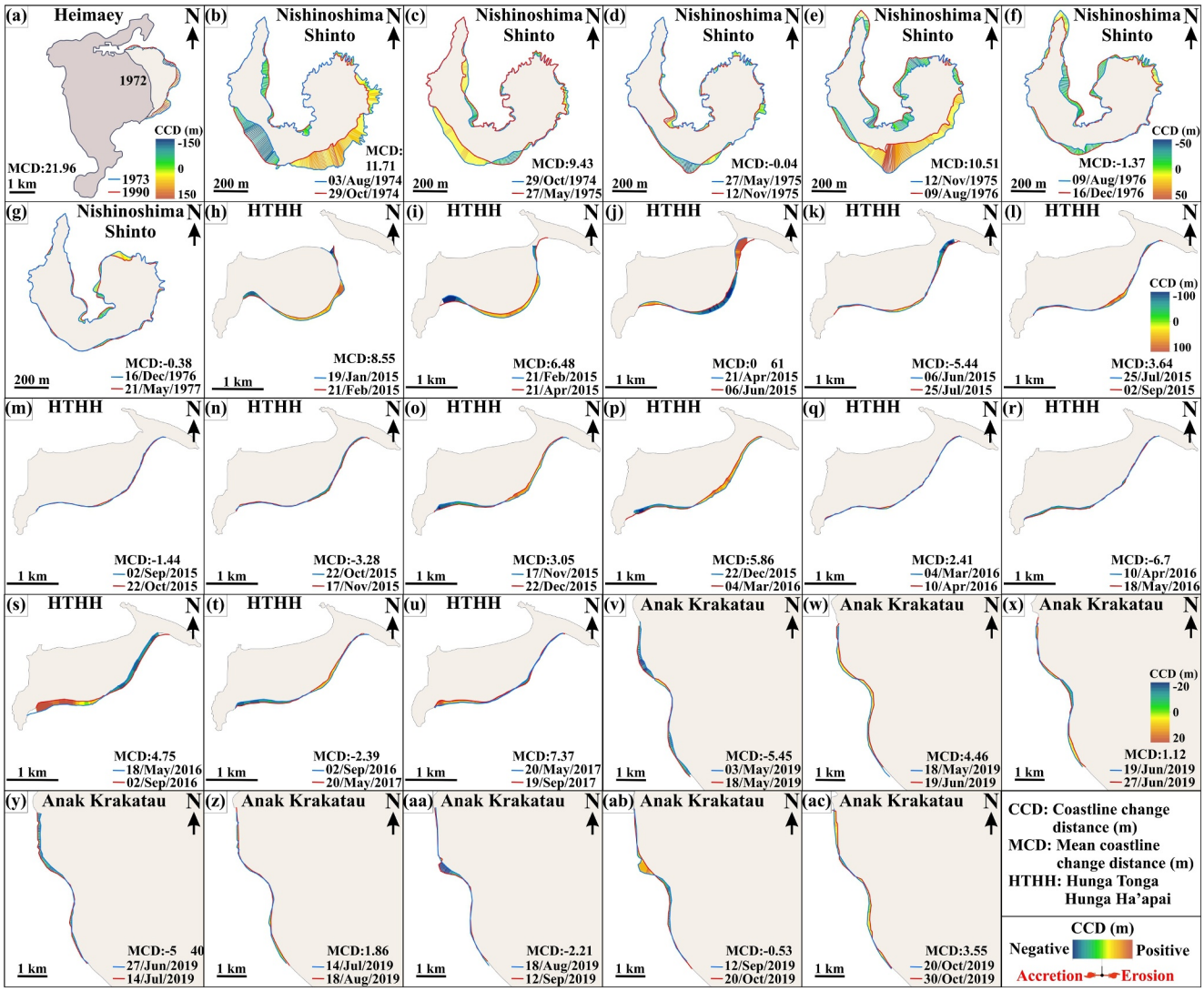

Figure 2. Coastline change distances for (a) Heimaey, (b–g) Nishinoshima Shinto, (h–u) Hunga Tonga Hunga Ha'apai and (v–ac) Anak Krakatau.

Deception Island where snowfall is prevalent (no attempt was made to separate rain and snow contributions). Tidal ranges (Figure 1a) were obtained from the FES2014 tidal model (https://www.aviso.altimetry.fr/en/data/products/auxiliary-products/global-tide-fes/description-fes2014.html). These environmental parameters were obtained from the ERA5 and tidal models at all 12 sites for consistency.

4. Results

4.1. Variations in ACR

ACR values vary significantly among the sites (Table S2 in Supporting Information S1), ranging from −376 m/yr (accreting) to +712 m/yr (eroding). The fastest retreat occurred at the north lava delta of La Palma, while its southern lava delta coast experienced the fastest accretion. ACR reached 100 m/yr on the coasts of Barcena, Capelinhos, Surtsey, Kasatochi and Anak Krakatau. In four cases, both erosion and accretion were witnessed after the eruption finished (Nishinoshima Shinto, Hunga Tonga Hunga Ha'apai, Anak Krakatau and La Palma).

ACR declined in magnitude generally with elapsed time (Mogi et al., 1980; Richards, 1965; Romagnoli & Jakobsson, 2015; Zhao et al., 2019), as illustrated by the two examples in Figure 3, though tephra coasts in Barcena and Anak Krakatau behaved differently (Table S2 in Supporting Information S1). At some sites, ACR modestly co-varies with MWH visually (Nishinoshima Shinto, La Palma north and south; Figure S4 in Supporting

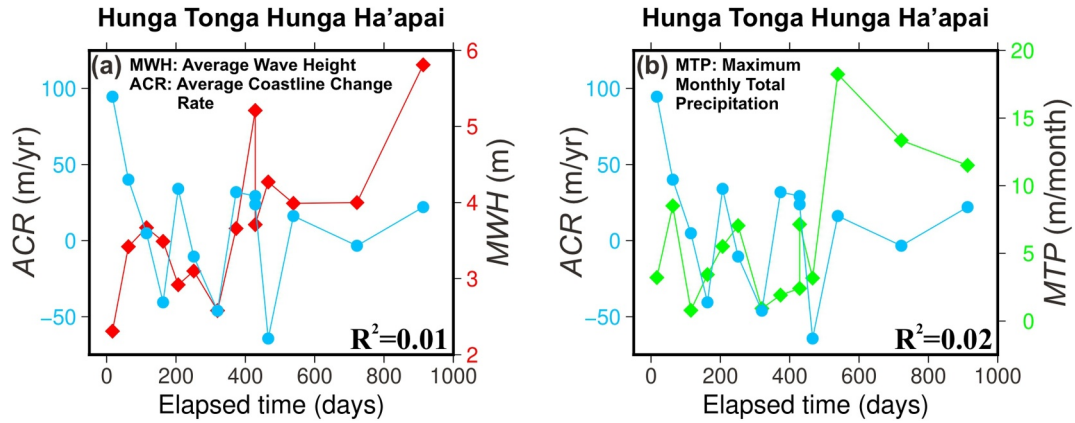

Figure 3. Examples of along-coast-averaged coastline change rates (ACR) of the volcanic coasts (blue lines) versus time since eruption. Negative values represent accretion. Also shown are (a) the maximum wave heights (MWH, red) and (b) the maximum monthly total precipitation (MTP, green) extracted from ERA5 (determined over the same time intervals as the ACR values). R^2 values were calculated between ACR and MWH (a) and between ACR and MTP (b). Similar graphs for other sites are shown in Figures S4 and S5 in Supporting Information S1.

Information S1). However, correlation coefficients (R^2) between ACR and MWH are generally modest (where more than two values were available) range from 0 to 0.60 with median 0.27 (Figure S4 in Supporting Information S1). In most cases, R^2 is smaller than 0.40, except at Surtsey, where R^2 was 0.60. Similarly, R^2 coefficients for variations with maximum MTP vary between 0 and 0.65, with a median value of 0.04 (Figure S5 in Supporting Information S1). At the rest of the sites, R^2 are <0.10, except at Capelinhos, Anak Krakatau and Surtsey, where R^2 is 0.65, 0.58 and 0.42, respectively. However, these seemingly reasonable correlations are actually negative, contradicting previous field observations (Young et al., 2009) and global relational database analyses (Prémaillon et al., 2018). Wave height and precipitation are hourly properties derived from ERA5 outputs; thus, they are reasonably useful for detecting extreme wave and rainfall events. Therefore, neither wave heights nor precipitation appear to control ACR strongly within this data set.

The highest ACR (HACR) value found at each site is shown in Table 2. The highest rates occurred soon after the eruptions, typically within 3 months. As episodicity of geomorphologic processes can affect erosion rate measurements (Gardner et al., 1987), we investigated the dependency of HACR on the time interval of each measurement. HACR values indeed decline with time interval (R^2 = 0.62, Figure 4a). The graph power-law slope resembles the trend for erosion of outcropping horizontal and sub-horizontal bedrock surfaces of Gingerich (2021), derived from ^{10}Be exposure dating (Portenga & Bierman, 2011). Therefore, episodicity of erosion has affected these values and likely also those in Figures S4 and S5 in Supporting Information S1. We also compared the HACR values with wave and rainfall parameters, finding little co-variation (R^2 = 0.20 and 0.00, Figures 4b and 4c). For a multivariate regression (Figure 4d), the R^2 value was slightly larger (0.24), suggesting some multivariate dependence of ACR. Nevertheless, the dependence is still weak.

4.2. Variations in ACD With Elapsed Time

We show model curve fits in Figure 5 even where few data exist as constraints as this allows us to estimate model parameters consistently for all sites for subsequent analysis. However, focusing first on the sites with more observations, where coastal evolution is known in more than 5 time steps (Figures 5b, 5e, 5f, 5h, 5k, 5n, and 5o) and in some cases less (Figures 5a, 5i and 5j), ACD values increased rapidly initially, then more slowly after typically ~10,000–20,000 days. The ACDs are well represented by Equation 8 for some individual sites with observations at multiple time steps (Figure 5; average R^2 = 0.89). This is also the case for grouped coasts (Figure 6; R^2: 0.91 to 1.00).

When fitting Equation 8 with varied α (Test 1), the α value found was mostly 0.5–3, with $\alpha = 3$ reached in Surtsey, Jadid and Tonga. The coefficient E_0 varies strongly between the sites (0.06–5.63 × 10^{10} day^{-1}). Between the different lithologies (Figure 6), E_0 and α vary within one order of magnitude. Mixed coasts are the exception, with E_0 of ~5,300 (day^{-1}).

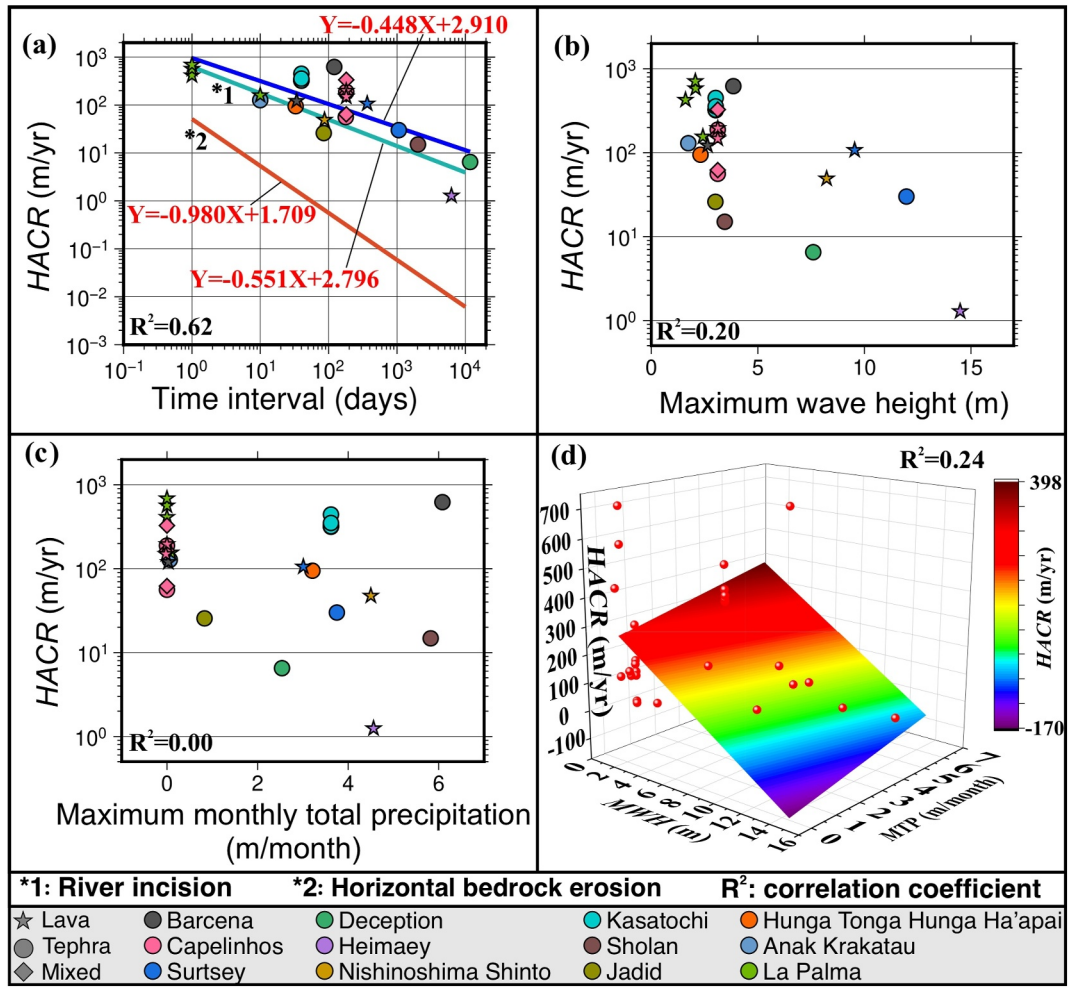

Figure 4. Highest average coastline retreat rates (HACR) for all coast types. (a) HACR versus measurement time interval plotted logarithmically. For comparison, green and red lines are inverse power law regressions of rates of change in rivers and horizontal bedrock erosion from Gingerich (2021). (b) HACR against the maximum wave height (MWH). (c) HACR against the local maximum monthly total precipitation (MTP). (d) Multi-variate regression of HACR on MWH and MTP.

When fitting Equation 8 with α set to 1.0 (Test 2), E_0 varied less strongly (0.16–79.66 days^{-1}). When grouped by lithology, E_0 only varies between 2.64 and 4.85 days^{-1}. Compared with the results with varied α (Test 1), letting $\alpha = 1.0$ appears to produce curves that have smaller ACD in the early stages and larger ACD in later stages (Figure 5). Correlation coefficients suggest a modestly better fitting of Equation 8 with varied α (Test 1) than fixed α (Test 2) in 90% of cases.

5. Discussion

The rates of coastline retreat tended to slow systematically (Figures 5 and 6). Here, we attempt to explain the variability of retreat rates and explore broader implications.

5.1. The Lack of Co-Variation of Waves and Precipitation Data With These Erosion Rates

Although wave height data were expected to co-vary with volcanic coastal retreat rates based on earlier observations (Menard, 1986; Quartau et al., 2010; Ramalho et al., 2013), Figure 4b reveals no such relationship. A lack of co-variation might arise from retreat rates varying with both measuring time intervals and elapsed times (i.e., a multiple dependency). To reduce the effect of temporal variability, we used the curve fitted to each ACD series to predict ACD (PACD; Table S3 in Supporting Information S1). The models with varied α were used (Test 1). However, PACDs computed for 100, 1,000 and 10,000 days also do not vary with wave heights (Figures 7a–7c).

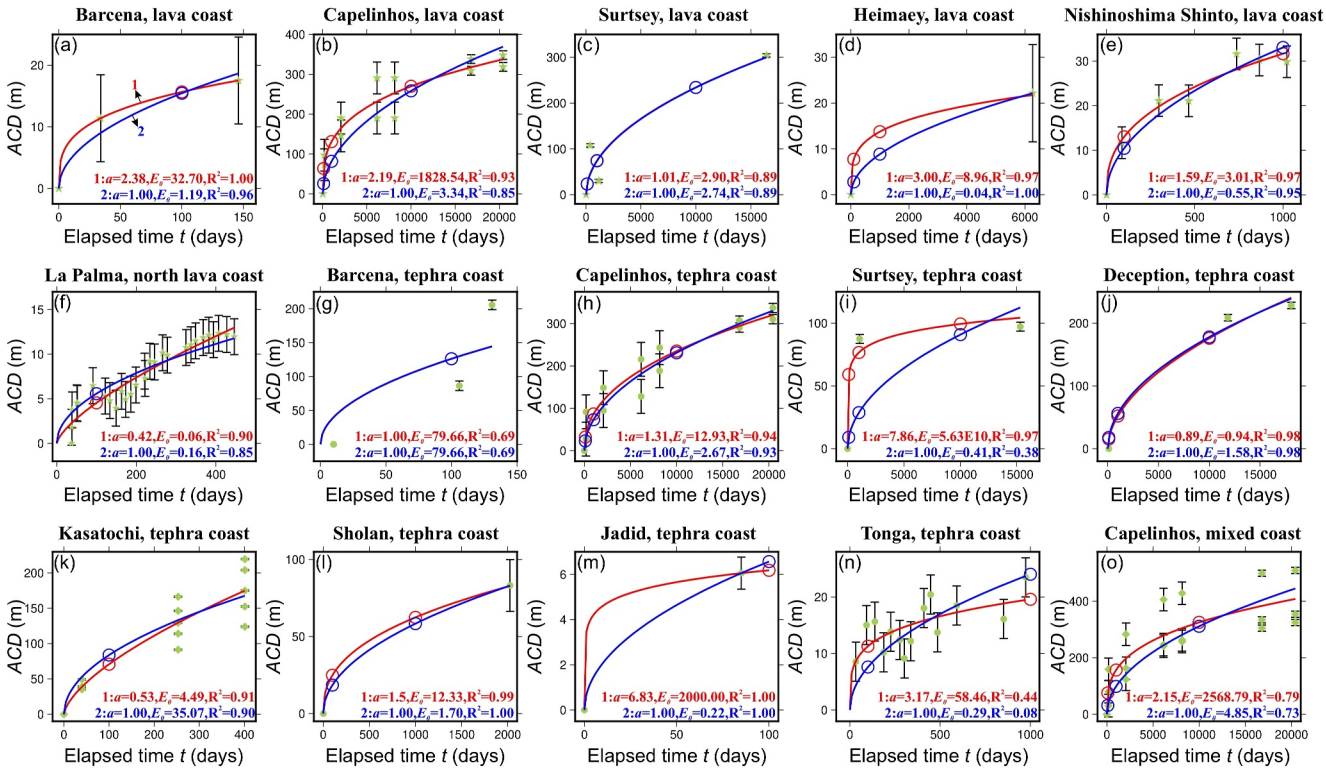

Figure 5. Accumulative coastline change distance (ACD) against elapsed time. Red and blue curves represent the least-squares best fits of Equation 8 to ACD with varied α (Test 1) and with α set to 1.0 (Test 2). Unfilled circles are estimated ACD values at t equal to 100, 1,000 and 10,000 days. Error bars indicate the estimated least total positional error in Table S1 in Supporting Information S1.

Precipitation can weaken sea cliffs through weathering (Duperret et al., 2005; Lim et al., 2010; Trenhaile, 2015) and elevated pore pressures can reduce effective stress on fractures, leading to cliff failures (Jakob & Lambert, 2009; Trenhaile, 2019). Therefore, retreat distances were expected to co-vary with precipitation (Young, 2018; Young et al., 2021). However, Figures 4c and 7d–7f show no relationship. In addition, exclusion of the Capelinhos data set did not improve correlations between Predicted accumulative coastline change distance and either wave height or precipitation, indicating that the absence of relationships is not due to the substantial Capelinhos dataset (Figures 7a–7f).

Perhaps the lack of co-variation arises from a dependence of erosion rates on multiple factors? For multivariate regressions (Figures 7g–7i), R^2 values are somewhat improved. However, the smallest HACR was observed for Heimaey despite experiencing strong waves and rainfall (Table 2). We calculated deviations of retreat distances from the predicted distances (using the fitted Equation 8 to remove the temporal systematic variation). The results in Figure S6 in Supporting Information S1 show only a modest R^2 when tested against wave and precipitation data.

A few effects may explain why the expected tendency was not found. First, the time lag of events may be important. for example, some coastlines of Hunga Tonga Hunga Ha'apai advanced during an interval of tall waves at 370 days (Figure 3), perhaps an effect of redistribution of sediment released by wave erosion. A similar effect was observed at Surtsey (Norrman & Erlingsson, 1992; Romagnoli & Jakobsson, 2015; Sayyadi et al., 2024). Furthermore, debris from cliff failures can advance coastlines before it is removed by waves. Second, precipitation on volcanic islands is strongly influenced by topographic effects (orography) (Ramalho et al., 2013) and taller islands have rain shadows. The lack of covariation could be due to the reliability and resolution of precipitation data derived from ERA5 outputs (Figure S3 in Supporting Information S1). However, the largest global cliff erosion database to date similarly revealed no covariation with climatic (temperature variation, frost frequency and precipitation) and marine (tidal range, wave energy flux and storm frequency) data (Prémaillon et al., 2018) data.

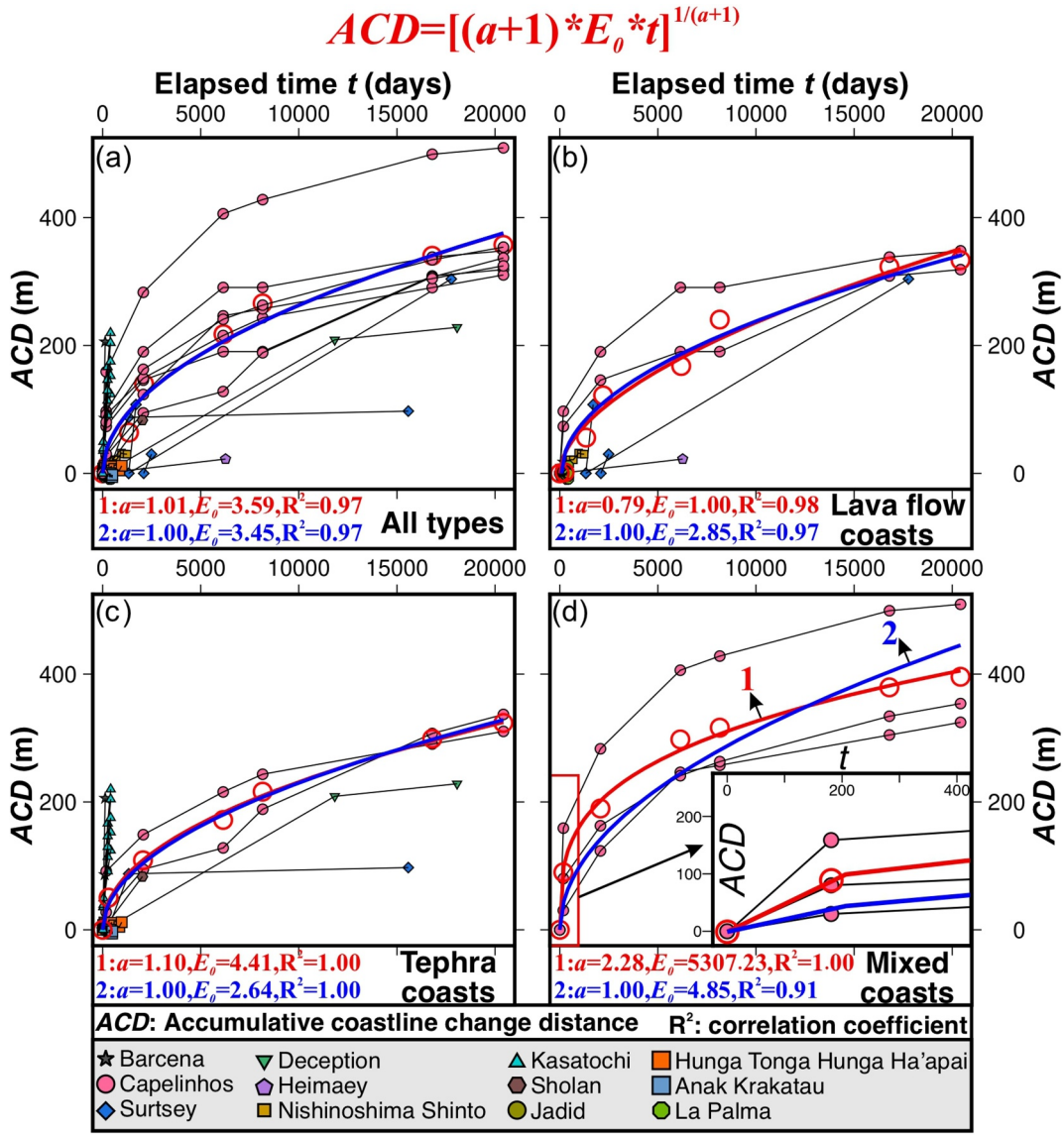

Figure 6. Accumulative coastline change distance (ACD) of all coastal types (a), lava flow (b), tephra (c) and mixed coasts (d). Unfilled red circles are ACD values averaged every ~1,000 days. Red and blue curves represent the least-squares best fit of Equation 8 to those averaged data with varied α (Test 1) and fixed α (Test 2). Notably, the red and blue curves overlap in panel (a). R^2 values represent the correlation coefficients when fitting observed data to the equation $ACD = [(a + 1)*E_0*t]^{1/(a+1)}$. The enlargement in (d) shows the changes in the early stages.

5.2. Other Factors Varying Coastal Erosion Rates

Tidal changes in water level also allow wave impacts to vary in position and magnitude through each tidal cycle (Bossis et al., 2025); however, no covariation was found between HACR and tidal range (Figure S7 in Supporting Information S1). Vertical tectonic movements may also vary coastal erosion rates (Quartau et al., 2018; Ramalho et al., 2013; Regard et al., 2010, 2021). Subsidence from compaction may accelerate erosion rates (Romagnoli & Jakobsson, 2015), while uplift during earthquakes may reduce them (Omidiji et al., 2022; Stephenson et al., 2017). Vertical motion data are available only for four of the 12 sites. These rates (all subsidence) are 1 cm/yr for Capelinhos (Catalão et al., 2006), 4 cm/yr for Surtsey (Romagnoli & Jakobsson, 2015), 1 cm/yr for Deception (Rosado et al., 2019), and 5 cm/yr for Anak Krakatau (Iqbal et al., 2023). These few rates also do not correlate with HACRs.

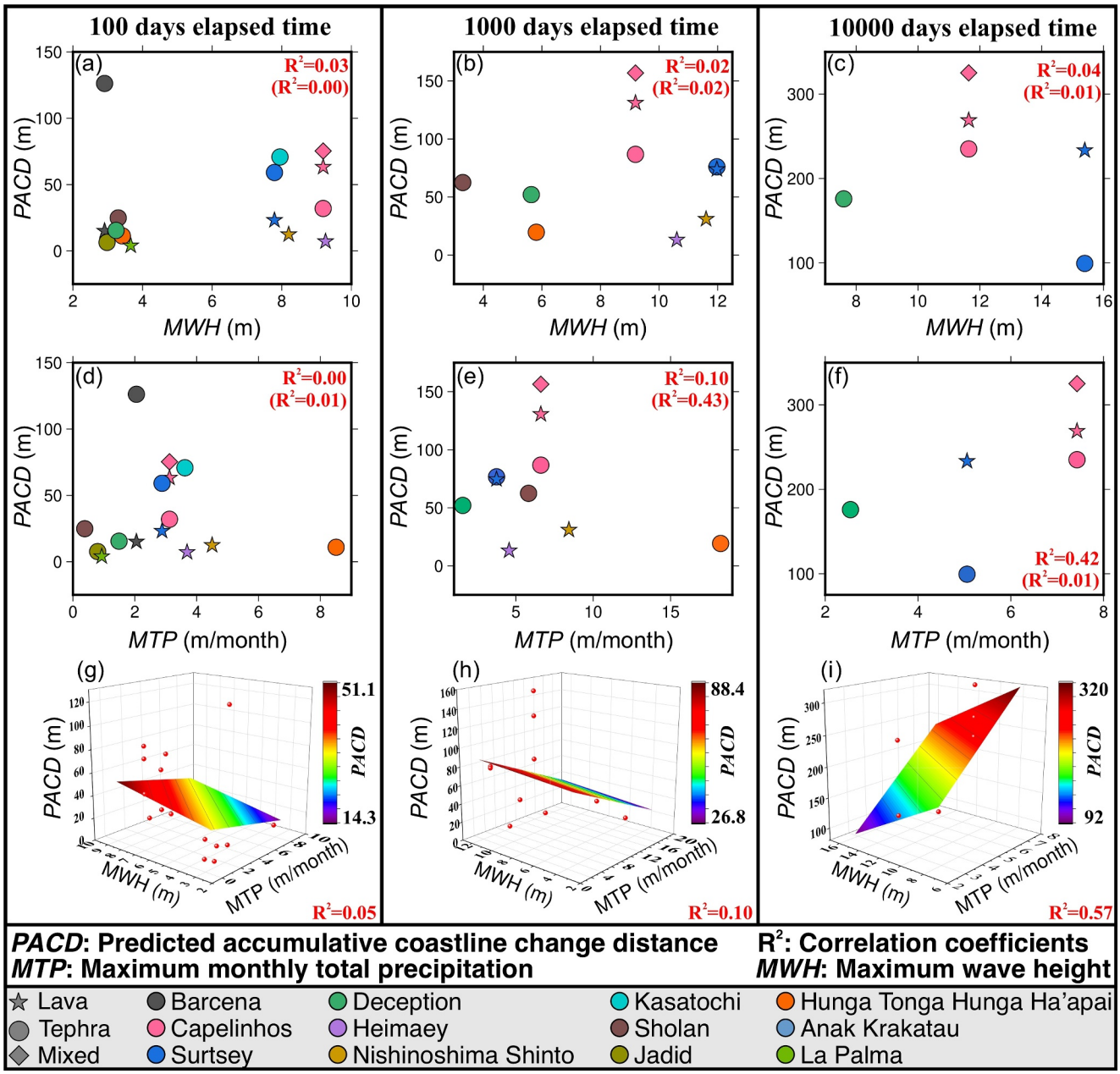

Figure 7. Predicted accumulative coastline change distance obtained by fitting Equation 8 with varied α to the ACD data. These are compared with (a–c) maximum wave height and (d–f) monthly total precipitation at elapsed time 100 days, 1,000 days and 10,000 days. Panels (g)–(i) show the results of multivariate regression. R^2 values in brackets are for analyses excluding the Capelinhos measurements.

A lava flows typically have interiors with low joint density, whereas pahoehoe flows have high joint densities (Smellie et al., 2013). Cavities and tube networks in pahoehoe lava flows allow water to enter cliffs during wave impacts (Macdonald, 1953), producing air compression effects (Andriani & Walsh, 2007; Zhao et al., 2020) and generating blow holes (Németh & Gravis, 2022). Hence, wave erosion should occur more rapidly at pahoehoe coasts than at a coasts. However, only one coast analyzed here comprises pahoehoe (Nishinoshima Shinto) and it did not erode more rapidly than most a lava flow coasts (Figure 5).

Prémaillon et al. (2018) suggested that variations in rock mass strength may primarily explain variations in erosion rates. Schmidt hammer measurements at Capelinhos showed unconfined compressive strengths (UCSs) of 51.6 MPa for lava flows, 22.4 MPa for mixed cliffs and 12.0 MPa for tephra cliffs (Zhao et al., 2019). These are

similar to UCSs of 52.75 and 23 MPa for volcanic and volcaniclastic rocks from a global rock strength database (https://doi.org/10.5281/zenodo.12687444). However, retreat rates do not follow a logical strength order, as mixed and lava flow coasts retreated more rapidly than weak tephra coasts (Figure 6).

Other properties may therefore be more important, such as fracture density (Kereszturi & Németh, 2012; Trenhaile, 2019). Such assessments are needed at these sites to further evaluate the effect of fracture density.

5.3. What Causes Erosion Rates to Decline Systematically With Measured Time Interval?

Uncertainties in long-term cliff retreat rates increase substantially with declining observation periods (Mushkin et al., 2019). Rapid alternating between coastal accretion and erosion can also affect time-averaged erosion rates depending on the averaging time interval (Castelle et al., 2018; Toimil et al., 2020). The covariation with time interval (Figure 4a) aligns with the results of Williams, Rosser, et al. (2019), who found that emplaced rockfall volume rates were higher for shorter intervals. Their power-law gradient ranged from −1.382 for 1-hr intervals to −0.995 for 1-month intervals, comparable to the −0.448 gradient in Figure 4a. Field measurements suggest that the reoccurrence period of cliff landslide episodes significantly influences rocky coastline change rates (Bloom et al., 2023; Mushkin et al., 2019).

Episodic and/or stochastic geomorphological processes are well-known to affect rates in general (Gardner et al., 1987; Rohmer & Dewez, 2013; Sadler & Jerolmack, 2015) and in individual volcanic coasts (Romagnoli & Jakobsson, 2015). The power-law slope of 0.448 is broadly comparable to those of denuding landscapes (0.815) (Gardner et al., 1987) and bedrock surface erosion (0.551) (Gingerich, 2021).

5.4. What Causes Erosion Rates to Decline Systematically With Elapsed Time?

We interpret the systematic slowing of retreat rates in Figure 6 as likely due to the combined effects of wave attenuation, protection by increasingly large debris bodies from cliff failures, and/or changes in exposed lithology (Zhao et al., 2019). Wave heights are reduced by attenuation crossing shore platforms in front of the cliffs (Sunamura, 1992; Trenhaile, 2000). As platforms widen with progressive coastal erosion (Matsumoto et al., 2016; Quartau et al., 2010, 2018; Ramalho et al., 2013), the heights of waves approaching cliffs should progressively decrease. Furthermore, volcanic islands, lava deltas and Surtseyan cones have conical shapes or part conical shapes (Francis, 1993; Macdonald et al., 2021). As coastlines retreat, these shapes lead to cliffs becoming progressively taller, resulting in larger debris fields from individual cliff failures. These debris fields can protect the cliff before they are removed by waves, thus slowing erosion (Zhao et al., 2019). Cliff heights are not known for the majority of the coasts analyzed here, but we were able to measure them from the digital elevation models (DEMs) of HTHH. In the results (Figure S8 in Supporting Information S1), coastline erosion rates decreased with increasing cliff height in seven of the 14 measurement periods, though with only modest R^2 values (0.06–0.45). This suggests that the blocking effect is less pronounced for tephra coasts.

Erosion may also progressively excavate more compacted or lithified material, which is more resistant to erosion (Ramalho et al., 2020; Zhao et al., 2019). For example, glass in deeper tuff at Surtsey was transformed into palagonite (Jakobsson et al., 2000). While palagonitization is unlikely to occur in rocks of common depths and therefore affect erosion rates in a common way, it and compaction may contribute to slowing at individual sites.

5.5. Potential for Geomorphologic Modeling

Over millions of years, abrasion shelf width can vary linearly with volcano age, suggesting that the width of a shelf may provide an estimate of the age of (reefless) coasts and the width of a guyot summit may suggest the longevity of the island that preceded it (Menard, 1984). Speciations among islands also depend on how long islands existed (Ávila et al., 2019; Geist et al., 2014; Whittaker & Hanski, 1999). Assuming linear changes in shelf widths over time would be inappropriate for the Pleistocene due to sea-level variations (Ramalho et al., 2013; Ricchi et al., 2018; Trenhaile, 2000). Retreat distances in our results also vary over short intervals (Figure 5). As we have not found a systematic variation with wave, precipitation and other data, we cannot correct for those factors. Hence, morphological dating does not appear promising over short timescales. However, other researchers have identified a strong relationship between shelf width and wave exposure (Bossis et al., 2023; Quartau et al., 2010, 2014, 2016; Romagnoli et al., 2018), suggesting that there is some systematic effect yet to be determined.

5.6. Implications for Coastal Management and Cliff Failure Hazards

New land produced by eruptions is appealing for touristic and agricultural development, although such development is discouraged (Poland & Orr, 2014). Predicting coastline retreat would be useful to place limits on development areas, as well as for assessing risks to geoheritage sites (Németh & Moufti, 2023). The systematic trends in Figures 5 and 6 may be useful for these purposes, that is, if those trends can be extrapolated into the future to predict how the coasts will change. Such extrapolations should not be viewed as deterministic, since the mechanisms causing coastal retreat rates to decrease are unclear and may change over time. Given also the variability of measurements, estimating future erosional risks solely through simple extrapolation would be problematic if only the initial rapid rates were considered. Only long-term rates in coasts approaching steady-state equilibria are likely to be accurate.

Cliff failure hazards is also need to be assessed in oceanic islands, which are typically remote from continental assistance (Shultz et al., 2016). The initially rapid retreats of their coasts can pose risks from cliff collapse (Mattox et al., 1993). Collapses are probably not so important volumetrically in young coasts because their cliffs are usually low. In contrast, failure of tall cliffs can initiate tsunamis that produce wider impacts (Omira, Baptista, et al., 2022; Rosser et al., 2013). Failures should become less frequent but more impactful as coasts retreat over time and cliffs become taller.

6. Conclusions

A data set has been compiled of post-eruptive coastal retreat rates for coasts formed by historical eruptions. It reveals a general tendency for rates to slow over time in the coasts recorded at multiple times. This slowing also results in accumulative coastline change distances (ACD) approaching equilibrium. The inverse power law variation between ACD and time is predictable from an earlier-found inverse power-law equation between retreat rate and retreat distance. Surprisingly, the anticipated influences of wave climate and precipitation have little correlation with these retreat rates. Covariations were also not observed with tidal range, subsidence rate, lava flow type, or rock strength. Differences in lithology and fracture density may dominate. The observed rates decrease with measurement time intervals, indicating that episodicity of erosion is important. The decline of rates with time elapsed since volcanic emplacement has been explained by (a) wave energy loss over widening shore platforms, (b) increasing resistance of more deeply buried materials becoming exposed at cliffs and (c) increasing volumes of debris generated by cliff collapses, given that volcanic land typically declines toward coasts. As a general tendency has been found in this study, the wave attenuation mechanism is likely the most important factor, as (b) and (c) likely produce less systematic effects. The general slowing tendency may be useful for managing newly formed volcanic coasts and for hazard assessment.

Acknowledgments
Z.Z. was supported by the National Natural Science Foundation of China (Grant 42206216), Guangdong Basic and Applied Basic Research Foundation (Grant 2025A1515012255), the Youth Talent Fund of the President of Chinese Academy of Sciences Guangzhou Branch (Grant 2023000352) and Guangzhou Basic and Applied Basic Research Foundation (Grant 2023A04J0205). We thank Cameron Hutton for preliminary exploration of the HTHH coastlines during his undergraduate project and for providing the La Palma coastline changes, which formed part of his dissertation. Many of our figures were produced with the free GMT software (https://www.generic-mapping-tools.org) (Wessel & Smith, 1995). This work was produced in synergy with project HAZARDOUS (PTDC/CTA-GEO/0798/2020) funded by the Portuguese Fundação para a Ciência e a Tecnologia (FCT) I.P./MCTES. Finally, we acknowledge constructive and helpful comments by the editor Ton Hoitink, Vincent Regard, Colin Bloom and an anonymous reviewer.

Data Availability Statement

Most of the coastline change distances were sourced from published studies (Hutton, 2023; Richards, 1965; Romagnoli et al., 2006; Torrecillas et al., 2024; Waythomas, Scott, Prejean, et al., 2010; Xu et al., 2015; Zhao et al., 2019). Historical coastline distances for Heimaey and Nishinoshima Shinto were obtained from published resources (Eiríksson, 1990; Mogi et al., 1980). Satellite images of Hunga Tonga Hunga Ha'apai are available in the supporting information of Garvin et al. (2018). Sentinel-2 satellite images for Anak Krakatau can be accessed from Novellino et al. (2020) and Google Earth Engine (Gorelick et al., 2017). Hourly significant wave height and total precipitation values can be extracted from the ERA5 database (Hersbach et al., 2023). Tidal range data can be obtained from the FES2014 tidal model (Lyard et al., 2021). Most figures were made with GMT software (Wessel et al., 2019, their version 6).

References

Abdurrachman, M., Widiyantoro, S., Priadi, B., & Ismail, T. (2018). Geochemistry and structure of krakatoa volcano in the Sunda Strait, Indonesia. *Geosciences*, *8*(4), 111. https://doi.org/10.3390/geosciences8040111

Aguirre, C., Rutllant, J. A., & Falvey, M. (2017). Wind waves climatology of the Southeast Pacific Ocean. *International Journal of Climatology*, *37*(12), 4288–4301. https://doi.org/10.1002/joc.5084

Alonso, I., Santana-Sarmiento, F. J., Andrés-Araujo, F., Casamayor, M., Montoya-Montes, I., Brenes, A., et al. (2023). Morphosedimentary characteristics and formation mechanisms of new beaches generated after the Tajogaite volcano eruption of 2021 (La Palma, Spain). *Marine Geology*, *462*, 107099. https://doi.org/10.1016/j.margeo.2023.107099

Andrade, C., Trigo, R., Freitas, M., Gallego, M., Borges, P., & Ramos, A. (2008). Comparing historic records of storm frequency and the North Atlantic Oscillation (NAO) chronology for the Azores region. *The Holocene*, *18*(5), 745–754. https://doi.org/10.1177/0959683608091794

Andriani, G. F., & Walsh, N. (2007). Rocky coast geomorphology and erosional processes: A case study along the Murgia coastline South of Bari, Apulia—SE Italy. *Geomorphology*, *87*(3), 224–238. https://doi.org/10.1016/j.geomorph.2006.03.033

Angulo-Preckler, C., Pernet, P., García-Hernández, C., Kereszturi, G., Álvarez-Valero, A. M., Hopfenblatt, J., et al. (2021). Volcanism and rapid sedimentation affect the benthic communities of Deception Island, Antarctica. *Continental Shelf Research*, *220*, 104404. https://doi.org/10.1016/j.csr.2021.104404

Arróspide, C., Aguilar, G., Martinod, J., Rodríguez, M. P., & Regard, V. (2023). Coastal cliff evolution: Modelling the long-term interplay between marine erosion, initial topography, and uplift in an arid environment. *Geomorphology*, *428*, 108642. https://doi.org/10.1016/j.geomorph.2023.108642

Ávila, S. P., Hipólito, A., Madeira, P., Baptista, L., Arruda, S., Castela Ávila, G., et al. (2023). On the geological and palaeontological Heritage of the azores Archipelago and the urgent need to review the geosites of the azores UNESCO geopark: A comment on Lima & meneses (2023), geoconservation research, 6: 114-127. *Geoconservation Research*, *6*(2). https://doi.org/10.57647/j.gcr.2023.0602.28

Ávila, S. P., Melo, C., Berning, B., Sá, N., Quartau, R., Rijsdijk, K. F., et al. (2019). Towards a "sea-level sensitive"dynamic model: Impact of island ontogeny and glacio-eustasy on global patterns of marine island biogeography. *Biological Reviews*, *94*(3), 1116–1142. https://doi.org/10.1111/brv.12492

Baba, K., Tada, N., Ichihara, H., Hamano, Y., Sugioka, H., Koyama, T., et al. (2020). Two independent signals detected by ocean bottom electromagnetometers during a non-eruptive volcanic event: Ogasawara Island arc volcano, Nishinoshima. *Earth Planets and Space*, *72*, 1–11. https://doi.org/10.1186/s40623-020-01240-z

Bandhauer, M., Isotta, F., Lakatos, M., Lussana, C., Båserud, L., Izsák, B., et al. (2022). Evaluation of daily precipitation analyses in E-OBS (v19.0e) and ERA5 by comparison to regional high-resolution datasets in European regions. *International Journal of Climatology*, *42*(2), 727–747. https://doi.org/10.1002/joc.7269

Bloom, C. K., Singeisen, C., Stahl, T., Howell, A., & Massey, C. (2023). Earthquake contributions to coastal cliff retreat. *Earth Surface Dynamics*, *11*(4), 757–778. https://doi.org/10.5194/esurf-11-757-2023

Bossis, R., Regard, V., & Carretier, S. (2023). Initial shape reconstruction of a volcanic island as a tool for quantifying long-term coastal erosion: The case of Corvo Island (Azores). *Earth Surface Dynamics*, *11*(3), 529–545. https://doi.org/10.5194/esurf-11-529-2023

Bossis, R., Regard, V., Carretier, S., & Choy, S. (2025). Evidence of slow millennial cliff retreat rates using cosmogenic nuclides in coastal colluvium. *Earth Surface Dynamics*, *13*(1), 71–79. https://doi.org/10.5194/esurf-13-71-2025

Brattstrom, B. H. (2015). Bárcena Volcano, 1952: A 60-year report on the repopulation of San Benedicto Island, Mexico, with a review of the ecological impacts of disastrous events. *Pacific Conservation Biology*, *21*(1), 38–59. https://doi.org/10.1071/PC14903

Brenna, M., Cronin, S. J., Smith, I. E., Pontesilli, A., Tost, M., Barker, S., et al. (2022). Post-caldera volcanism reveals shallow priming of an intra-ocean arc andesitic caldera: Hunga volcano, Tonga, SW Pacific. *Lithos*, *412*, 106614. https://doi.org/10.1016/j.lithos.2022.106614

Carracedo, J. C., Troll, V. R., Day, J. M., Geiger, H., Aulinas, M., Soler, V., et al. (2022). The 2021 eruption of the cumbre vieja volcanic ridge on la palma, canary islands. *Geology Today*, *38*(3), 94–107. https://doi.org/10.1111/gto.12388

Carvalho, F. (2003). *Elementos do clima de agitação marítima no grupo central dos Açores* (Vol. 97). Instituto de Meteorologia.

Castelle, B., Guillot, B., Marieu, V., Chaumillon, E., Hanquiez, V., Bujan, S., & Poppeschi, C. (2018). Spatial and temporal patterns of shoreline change of a 280-km high-energy disrupted sandy coast from 1950 to 2014: SW France. *Estuarine, Coastal and Shelf Science*, *200*, 212–223. https://doi.org/10.1016/j.ecss.2017.11.005

Catalão, J., Miranda, J., & Lourenço, N. (2006). Deformation associated with the Faial (Capelinhos) 1957–1958 eruption: Inferences from 1937–1997 geodetic measurements. *Journal of Volcanology and Geothermal Research*, *155*(3–4), 151–163. https://doi.org/10.1016/j.jvolgeores.2006.03.028

Clare, M. A., Yeo, I. A., Watson, S., Wysoczanski, R., Seabrook, S., Mackay, K., et al. (2023). Fast and destructive density currents created by ocean-entering volcanic eruptions. *Science*, *381*(6662), 1085–1092. https://doi.org/10.1126/science.adi3038

Claudino-Sales, V. (2019). Ogasawara Islands, Japan, In *Coastal world heritage sites* (pp. 341–347). Springer. https://doi.org/10.1007/978-94-024-1528-5_50

Cole, P., Guest, J., Duncan, A., & Pacheco, J.-M. (2001). Capelinhos 1957–1958, Faial, Azores: Deposits formed by an emergent surtseyan eruption. *Bulletin of Volcanology*, *63*(2–3), 204–220. https://doi.org/10.1007/s004450100136

Coutinho, R. (2000). Elementos para a monitorização sismovulcânica da ilha do Faial (Açores): caracterização hidrogeológica e avaliação de anomalias de Rn associadas a fenómenos de desgaseificação, Universidade dos Açores, Ponta Delgada.

Del Fresno, C., Cesca, S., Klügel, A., Domínguez Cerdeña, I., Díaz-Suárez, E. A., Dahm, T., et al. (2023). Magmatic plumbing and dynamic evolution of the 2021 La Palma eruption. *Nature Communications*, *14*(1), 358. https://doi.org/10.1038/s41467-023-35953-y

Deplus, C., Bonvalot, S., Dahrin, D., Diament, M., Harjono, H., & Dubois, J. (1995). Inner structure of the Krakatau volcanic complex (Indonesia) from gravity and bathymetry data. *Journal of Volcanology and Geothermal Research*, *64*(1–2), 23–52. https://doi.org/10.1016/0377-0273(94)00038-I

Duperret, A., Taibi, S., Mortimore, R. N., & Daigneault, M. (2005). Effect of groundwater and sea weathering cycles on the strength of chalk rock from unstable coastal cliffs of NW France. *Engineering Geology*, *78*(3–4), 321–343. https://doi.org/10.1016/j.enggeo.2005.01.004

Eiríksson, J. (1990). Clast shape development on a new lava beach at the Heimaey harbour, Iceland. *Journal of Coastal Research*, 486–506.

Etienne, S., & Paris, R. (2010). Boulder accumulations related to storms on the south coast of the Reykjanes Peninsula (Iceland). *Geomorphology*, *114*(1–2), 55–70. https://doi.org/10.1016/j.geomorph.2009.02.008

Ferrer, N., Marrero-Rodríguez, N., Sanromualdo-Collado, A., Vegas, J., & García-Romero, L. (2023). Early morphodynamics of the sudden formation of beaches during the 2021 volcanic eruption of La Palma. *Geomorphology*, *436*, 108779. https://doi.org/10.1016/j.geomorph.2023.108779

Ferrer-Valero, N., Hernández-Calvento, L., & Hernández-Cordero, A. I. (2019). Insights of long-term geomorphological evolution of coastal landscapes in hot-spot oceanic islands. *Earth Surface Processes and Landforms*, *44*(2), 565–580. https://doi.org/10.1002/esp.4518

Fiantis, D., Ginting, F., Gusnidar, Nelson, M., Van Ranst, E., & Minasny, B. (2021). Geochemical characterization and evolution of soils from Krakatau Islands. *Eurasian Soil Science*, *54*(11), 1629–1643. https://doi.org/10.1134/S1064229321110077

Fletcher, C. H., Romine, B. M., Genz, A. S., Barbee, M. M., Dyer, M., Anderson, T. R., et al. (2012). *National assessment of shoreline change: Historical shoreline change in the Hawaiian Islands*. U.S. Geological Survey Open-File Report 2011–1051 *Rep*.55.

Forjaz, V. H. (2004). Atlas Básico dos Açores, Obs. Vulcanológico e Geotérmico dos Açores, Ponta Delgada.

Forjaz, V. H. (2007). Vulcão dos Capelinhos: memórias 1957–2007, Observatório Vulcanológico e Geotérmico dos Açores: Portugal., Ponta Delgada.

Francis, P. (1993). *Volcanoes. A planetary perspective*. Oxford University Press.

Gardner, T. W., Jorgensen, D. W., Shuman, C., & Lemieux, C. R. (1987). Geomorphic and tectonic process rates: Effects of measured time interval. *Geology*, *15*(3), 259–261. https://doi.org/10.1130/0091-7613(1987)15<259:GATPRE>2.0.CO;2

Garvin, J. B., Slayback, D. A., Ferrini, V., Frawley, J., Giguere, C., Asrar, G. R., & Andersen, K. (2018). Monitoring and modeling the rapid evolution of Earth's newest volcanic island: Hunga Tonga Hunga Ha'apai (Tonga) using high spatial resolution satellite observations. *Geophysical Research Letters*, *45*(8), 3445–3452. https://doi.org/10.1002/2017GL076621

Geist, D. J., Snell, H., Snell, H., Goddard, C., & Kurz, M. D. (2014). A paleogeographic model of the Galápagos Islands and biogeographical and evolutionary implications, In *The Galápagos: A natural laboratory for the Earth sciences* (pp. 145–166). John Wiley and Sons. https://doi.org/10.1002/9781118852538.ch8

Geyer, A., Pedrazzi, D., Almendros, J., Berrocoso, M., López-Martínez, J., Maestro, A., et al. (2021). Deception Island. In *Volcanism in Antarctica: 200 million years of subduction, rifting and Continental Break-up*. Geological Society of London. https://doi.org/10.1144/M55-2018-56

Gingerich, P. D. (2021). Rates of geological processes. *Earth-Science Reviews*, *220*, 103723. https://doi.org/10.1016/j.earscirev.2021.103723

Gonçalves, M., Martinho, P., & Soares, C. G. (2020). Wave energy assessment based on a 33-year hindcast for the Canary Islands. *Renewable Energy*, *152*, 259–269. https://doi.org/10.1016/j.renene.2020.01.011

González, P. J. (2022). Volcano-tectonic control of Cumbre Vieja. *Science*, *375*(6587), 1348–1349. https://doi.org/10.1126/science.abn5148

Gorelick, N., Hancher, M., Dixon, M., Ilyushchenko, S., Thau, D., & Moore, R. (2017). Google Earth Engine: Planetary-scale geospatial analysis for everyone [Software]. *Remote Sensing of Environment*, *202*, 18–27. https://doi.org/10.1016/j.rse.2017.06.031

Hall, A. M., Hansom, J. D., & Jarvis, J. (2008). Patterns and rates of erosion produced by high energy wave processes on hard rock headlands: The grind of the Navir, Shetland, Scotland. *Marine Geology*, *248*(1–2), 28–46. https://doi.org/10.1016/j.margeo.2007.10.007

Hansom, J. D., Forbes, D., & Etienne, S. (2014). Chapter 16 the rock coasts of polar and sub-polar regions. *Geological Society, London, Memoirs*, *40*(1), 263–281. https://doi.org/10.1144/M40.16

Hasanean, H., & Almazroui, M. (2015). Rainfall: Features and variations over Saudi Arabia, a review. *Climate*, *3*(3), 578–626. https://doi.org/10.3390/cli3030578

Hersbach, H., Bell, B., Berrisford, P., Biavati, G., Horányi, A., Muñoz Sabater, J., et al. (2023). ERA5 hourly data on single levels from 1940 to present [Dataset]. *Copernicus Climate Change Service (C3S) Climate Data Store (CDS)*. https://doi.org/10.24381/cds.adbb2d47

Huppert, K. L., Perron, J. T., & Ashton, A. D. (2020). The influence of wave power on bedrock sea-cliff erosion in the Hawaiian Islands. *Geology*, *48*(5), 499–503. https://doi.org/10.1130/G47113.1

Hutton, C. (2023). *Coastal erosion around hunga Tonga Hunga Ha'apai (HTHH) before it erupted*. University of Manchester.83.

Iqbal, M., Denhi, A. D. A., & Prayoga, A. (2023). Morphological analysis of Anak Krakatau Volcano after 22 December 2018 eruption using differential interferometry synthetic aperture radar (DInSAR). *Journal of Geoscience, Engineering, Environment, and Technology*, *8*(2), 90–98. https://doi.org/10.25299/jgeet.2023.8.2.11651

Jakob, M., & Lambert, S. (2009). Climate change effects on landslides along the southwest coast of British Columbia. *Geomorphology*, *107*(3–4), 275–284. https://doi.org/10.1016/j.geomorph.2008.12.009

Jakobsson, S. P. (1972). On the consolidation and palagonitization of the tephra of the Surtsey volcanic island, Iceland. *Surtsey Progress Report*, *6*, 1.

Jakobsson, S. P., Gudmundsson, G., & Moore, J. G. (2000). Geological monitoring of Surtsey, Iceland, 1967-1998. *Surtsey Research*, *11*, 99–108. https://doi.org/10.33112/surtsey.11.13

Jiang, Q., Li, W., Fan, Z., He, X., Sun, W., Chen, S., et al. (2021). Evaluation of the ERA5 reanalysis precipitation dataset over Chinese Mainland. *Journal of hydrology*, *595*, 125660. https://doi.org/10.1016/j.jhydrol.2020.125660

Jones, E. V., Rosser, N., Brain, M., & Petley, D. (2015). Quantifying the environmental controls on erosion of a hard rock cliff. *Marine Geology*, *363*, 230–242. https://doi.org/10.1016/j.margeo.2014.12.008

Jónsson, S., & Xu, W. (2015). Volcanic eruptions in the southern Red Sea during 2007–2013, In *The Red Sea: The formation, morphology, oceanography and environment of a young ocean basin* (pp. 175–186). Springer. https://doi.org/10.1007/978-3-662-45201-1_10

Kereszturi, G., & Németh, K. (2012). Structural and morphometric irregularities of eroded Pliocene scoria cones at the Bakony–Balaton highland volcanic field, Hungary. *Geomorphology*, *136*(1), 45–58. https://doi.org/10.1016/j.geomorph.2011.08.005

Kudo, T., & Hoshizumi, H. (2006). Catalog of eruptive events within the last 10,000 years in Japan, database of Japanese active volcanoes. In *Geol surv Japan, AIST*.

Lasky, K. (2012). *Surtsey: The newest place on Earth*. StarWalk Kids Media.

Li, R., Wu, K., Zhang, W., Dong, X., Lv, L., Li, S., et al. (2023). Analysis of the 20-Year variability of ocean wave hazards in the northwest Pacific. *Remote Sensing*, *15*(11), 2768. https://doi.org/10.3390/rs15112768

Lim, M., Rosser, N. J., Allison, R. J., & Petley, D. N. (2010). Erosional processes in the hard rock coastal cliffs at Staithes, North Yorkshire. *Geomorphology*, *114*(1–2), 12–21. https://doi.org/10.1016/j.geomorph.2009.02.011

Lipman, P. W., & Moore, J. G. (1996). Mauna Loa lava accumulation rates at the Hilo drill site: Formation of lava deltas during a period of declining overall volcanic growth. *Journal of Geophysical Research*, *101*(B5), 11631–11641. https://doi.org/10.1029/95JB03214

Lonin, S., Rios-Angulo, W. A., & Coronado, J. (2022). Swell conditions at potential sites for the Colombian Antarctic research station. *Sustainability*, *14*(4), 2318. https://doi.org/10.3390/su14042318

Lyard, F. H., Allain, D. J., Cancet, M., Carrère, L., & Picot, N. (2021). FES2014 global ocean tide atlas: Design and performance. *Ocean Science*, *17*(3), 615–649. [Model]. https://doi.org/10.5194/os-17-615-2021

Macdonald, G. A. (1953). Pahoehoe, aa, and block lava. *American Journal of Science*, *251*(3), 169–191. https://doi.org/10.2475/ajs.251.3.169

Macdonald, G. A., Abbott, A., & Peterson, F. L. (2021). *Volcanoes in the sea: The geology of Hawaii*. University of Hawaii press.

Machado, F., Nascimento, J., & Denis, A. (1959). Evolução topográfica do cone vulcânico dos Capelinhos. *Serv Geol Port Mere*, *4*, 65–67.

Machado, F., Parsons, W. H., Richards, A. F., & Mulford, J. W. (1962). Capelinhos eruption of Fayal volcano, Azores, 1957–1958. *Journal of Geophysical Research*, *67*(9), 3519–3529. https://doi.org/10.1029/JZ067i009p03519

Madeira, J. (2007). A erupção dos Capelinhos e o vulcanismo nos Açores. *Boletim do Núcleo Cultural da Horta*, *16*, 29–44.

Madeira, J., Brum da Silveira, A., Hipólito, A., & Carmo, R. (2015). Chapter 3 active tectonics in the central and eastern Azores islands along the Eurasia–Nubia boundary: A review. *Geological Society, London, Memoirs*, *44*(1), 15–32. https://doi.org/10.1144/M44.3

Matsumoto, H., Dickson, M., Stephenson, W., Thompson, C., & Young, A. (2024). Modeling future cliff-front waves during sea level rise and implications for coastal cliff retreat rates. *Scientific Reports*, *14*(1), 7810. https://doi.org/10.1038/s41598-024-57923-0

Matsumoto, H., Dickson, M. E., & Kench, P. S. (2016). An exploratory numerical model of rocky shore profile evolution. *Geomorphology*, *268*, 98–109. https://doi.org/10.1016/j.geomorph.2016.05.017

Mattox, T. N., Heliker, C., Kauahikaua, J., & Hon, K. (1993). Development of the 1990 Kalapana flow field, Kilauea volcano, Hawaii. *Bulletin of Volcanology*, *55*(6), 407–413. https://doi.org/10.1007/BF00302000

Mattsson, H., & Höskuldsson, Á. (2003). Geology of the Heimaey volcanic centre, south Iceland: Early evolution of a central volcano in a propagating rift? *Journal of Volcanology and Geothermal Research*, *127*(1–2), 55–71. https://doi.org/10.1016/S0377-0273(03)00178-1

Menard, H. (1984). Origin of guyots: The Beagle to Seabeam. *Journal of Geophysical Research*, *89*(B13), 11117–11123. https://doi.org/10.1029/JB089iB13p11117

Menard, H. (1986). *Islands*. Scientific American Library.230.

Mogi, A., Tsuchide, M., & Mori, T. (1980). Growth process of a new volcanic island investigated by remote sensing method. *Marine Geodesy*, *4*(3), 249–265. https://doi.org/10.1080/15210608009379387

Morgan, A. V. (2000). The Eldfell eruption, Heimaey, Iceland: A 25-year retrospective. *Geoscience Canada*. https://doi.org/10.12789/gs.v27i1.4030

Moses, C., & Robinson, D. (2011). Chalk coast dynamics: Implications for understanding rock coast evolution. *Earth-Science Reviews*, *109*(3–4), 63–73. https://doi.org/10.1016/j.earscirev.2011.08.003

Mushkin, A., Katz, O., & Porat, N. (2019). Overestimation of short-term coastal cliff retreat rates in the eastern Mediterranean resolved with a sediment budget approach. *Earth Surface Processes and Landforms*, *44*(1), 179–190. https://doi.org/10.1002/esp.4490

Naylor, L., & Stephenson, W. (2010). On the role of discontinuities in mediating shore platform erosion. *Geomorphology*, *114*(1–2), 89–100. https://doi.org/10.1016/j.geomorph.2008.12.024

Németh, K., Cronin, S. J., Charley, D., Harrison, M., & Garae, E. (2006). Exploding lakes in Vanuatu: "Surtseyan-style"eruptions witnessed on Ambae Island. https://doi.org/10.18814/epiiugs/2006/v29i2/002

Németh, K., & Gravis, I. (2022). Geoheritage and geodiversity elements of the SW Pacific: A conceptual framework. *International Journal of Geoheritage and Parks*, *10*(4), 523–545. https://doi.org/10.1016/j.ijgeop.2022.09.001

Németh, K., & Moufti, M. R. (2023). Lava flow hazard and its implication in geopark development for the active Harrat khaybar intracontinental monogenetic volcanic field, Saudi Arabia. *Land*, *12*(3), 705. https://doi.org/10.3390/land12030705

Norrman, J. O. (1978). *Coastal changes in surtsey Island* (Vol. 1972–1975, pp. 53–59). The Surtsey Research Society.

Norrman, J. O. (1972). *Coastal changes in surtsey Island* (Vol. 1969–1970, pp. 145–149). The Surtsey Research Society.

Norrman, J. O. (1985). Stages of coastal development in Surtsey island, Iceland. In *Paper presented at proceedings of the Iceland coastal and river symposium*.

Norrman, J. O., & Erlingsson, U. (1992). The submarine morphology of Surtsey volcanic group. *Surtsey Research Progress Report*, *10*, 45–56. https://doi.org/10.33112/surtsey.10.6

Novellino, A., Engwell, S. L., Grebby, S., Day, S., Cassidy, M., Madden-Nadeau, A., et al. (2020). Mapping recent shoreline changes spanning the lateral collapse of Anak Krakatau Volcano, Indonesia. *Applied Sciences*, *10*(2), 536. https://doi.org/10.3390/app10020536

Omidiji, J., Stephenson, W., Dickson, M., & Norton, K. (2022). Tectonics and shore platform development: Rates and patterns of erosion on recently uplifted mudstone and limestone rocks at Kaikōura Peninsula, New Zealand. *Marine Geology*, *451*, 106887. https://doi.org/10.1016/j.margeo.2022.106887

Omira, R., Baptista, M., Quartau, R., Ramalho, R., Kim, J., Ramalho, I., & Rodrigues, A. (2022). How hazardous are tsunamis triggered by small-scale mass-wasting events on volcanic islands? New insights from Madeira–NE Atlantic. *Earth and Planetary Science Letters*, *578*, 117333. https://doi.org/10.1016/j.epsl.2021.117333

Omira, R., Ramalho, R., Kim, J., González, P. J., Kadri, U., Miranda, J., et al. (2022b). Global Tonga tsunami explained by a fast-moving atmospheric source. *Nature*, *609*(7928), 734–740. https://doi.org/10.1038/s41586-022-04926-4

Pedrazzi, D., Aguirre-Díaz, G., Bartolini, S., Martí, J., & Geyer, A. (2014). The 1970 eruption on Deception Island (Antarctica): Eruptive dynamics and implications for volcanic hazards. *Journal of the Geological Society*, *171*(6), 765–778. https://doi.org/10.1144/jgs2014-015

Pérez, V., Larrañaga, N., Abdallah, D., Wünsch, A., & Hormaza, J. I. (2020). Genetic diversity of local peach (Prunus persica) accessions from La Palma island (Canary Islands, Spain). *Agronomy*, *10*(4), 457. https://doi.org/10.3390/agronomy10040457

Petersen, G. N., & Jónsson, T. (2020). The climate of Surtsey. *Surtsey Research*, *14*, 9–16. https://doi.org/10.33112/surtsey.14.1

Phillips, J. D. (2006). Evolutionary geomorphology: Thresholds and nonlinearity in landform response to environmental change. *Hydrology and Earth System Sciences*, *10*(5), 731–742. https://doi.org/10.5194/hess-10-731-2006

Poland, M. P., & Orr, T. R. (2014). Identifying hazards associated with lava deltas. *Bulletin of Volcanology*, *76*(12), 1–10. https://doi.org/10.1007/s00445-014-0880-0

Portenga, E. W., & Bierman, P. R. (2011). Understanding Earth's eroding surface with ^{10}Be. *Geological Society of America Today*, *21*(8), 4–10. https://doi.org/10.1130/G111A.1

Prémaillon, M., Regard, V., Dewez, T. J., & Auda, Y. (2018). GlobR2C2 (global recession rates of coastal cliffs): A global relational database to investigate coastal rocky cliff erosion rate variations. *Earth Surface Dynamics*, *6*(3), 651–668. https://doi.org/10.5194/esurf-6-651-2018

Putnam, W. C., Axelrod, D. I., Bailey, H. P., & MvGill, J. T. (1960). *Natural coastal environments of the world*. University of California.

Quartau, R., Hipólito, A., Romagnoli, C., Casalbore, D., Madeira, J., Tempera, F., et al. (2014). The morphology of insular shelves as a key for understanding the geological evolution of volcanic islands: Insights from Terceira Island (Azores). *Geochemistry, Geophysics, Geosystems*, *15*(5), 1801–1826. https://doi.org/10.1002/2014GC005248

Quartau, R., Madeira, J., Mitchell, N., Tempera, F., Silva, P., & Brandão, F. (2016). Reply to comment by Marques et al. on "The insular shelves of the Faial-Pico Ridge (Azores archipelago): A morphological record of its evolution". *Geochemistry, Geophysics, Geosystems*, *17*(2), 633–641. https://doi.org/10.1002/2015gc006180

Quartau, R., Trenhaile, A., Mitchell, N., & Tempera, F. (2010). Development of volcanic insular shelves: Insights from observations and modelling of Faial Island in the Azores Archipelago. *Marine Geology*, *275*(1–4), 66–83. https://doi.org/10.1016/j.margeo.2010.04.008

Quartau, R., Trenhaile, A. S., Ramalho, R. S., & Mitchell, N. C. (2018). The role of subsidence in shelf widening around ocean island volcanoes: Insights from observed morphology and modeling. *Earth and Planetary Science Letters*, *498*, 408–417. https://doi.org/10.1016/j.epsl.2018.07.007

Ramalho, R. S., Quartau, R., Hóskuldsson, Á., Madeira, J., da Cruz, J. V., & Rodrigues, A. (2020). Evidence for late Pleistocene volcanism at Santa Maria Island, Azores? *Journal of Volcanology and Geothermal Research*, *394*, 106829. https://doi.org/10.1016/j.jvolgeores.2020.106829

Ramalho, R. S., Quartau, R., Trenhaile, A. S., Mitchell, N. C., Woodroffe, C. D., & Ávila, S. P. (2013). Coastal evolution on volcanic oceanic islands: A complex interplay between volcanism, erosion, sedimentation, sea-level change and biogenic production. *Earth-Science Reviews*, *127*, 140–170. https://doi.org/10.1016/j.earscirev.2013.10.007

Regard, V., Martinod, J., Saillard, M., Carretier, S., Leanni, L., Hérail, G., et al. (2021). Late Miocene-Quaternary forearc uplift in southern Peru: New insights from ^{10}Be dates and rocky coastal sequences. *Journal of South American Earth Sciences*, *109*, 103261. https://doi.org/10.1016/j.jsames.2021.103261

Regard, V., Saillard, M., Martinod, J., Audin, L., Carretier, S., Pedoja, K., et al. (2010). Renewed uplift of the Central Andes Forearc revealed by coastal evolution during the Quaternary. *Earth and Planetary Science Letters*, *297*(1–2), 199–210. https://doi.org/10.1016/j.epsl.2010.06.020

Ricchi, A., Quartau, R., Ramalho, R. S., Romagnoli, C., Casalbore, D., da Cruz, J. V., et al. (2018). Marine terrace development on reefless volcanic islands: New insights from high-resolution marine geophysical data offshore Santa Maria Island (Azores Archipelago). *Marine Geology*, *406*, 42–56. https://doi.org/10.1016/j.margeo.2018.09.002

Richards, A. F. (1961). *Rates of marine erosion of tephra and lava at Isla San Benedicto, Mexico*. University of California, Scripps Institution of Oceanography.

Richards, A. F. (1965). Geology of the islas revillagigedo, 3. Effects of erosion on isla San Benedicto 1952–61 following the birth of Volcán Bárcena. *Bulletin Volcanologique*, *28*(1), 381–403. https://doi.org/10.1007/BF02596940

Richards, A. F. (1966). Geology of the Islas Revillagigedo, México: 2. Geology and petrography of Isla San Benedicto. In *Proceedings of the California Academy of sciences* (pp. 361–414).

Richards, A. F., & Brattstrom, B. H. (1959). Bibliography, cartography, discovery and exploration of the Islas Revillagigedo. In *Proceedings of the California academy of sciences* (pp. 315–360).

Rodionov, S. N., Overland, J. E., & Bond, N. A. (2005). Spatial and temporal variability of the Aleutian climate. *Fisheries Oceanography*, *14*(s1), 3–21. https://doi.org/10.1111/j.1365-2419.2005.00363.x

Rodriguez-Gonzalez, A., Fernandez-Turiel, J., Aulinas, M., Cabrera, M., Prieto-Torrell, C., Rodriguez, G., et al. (2022). Lava deltas, a key landform in oceanic volcanic islands: El Hierro, Canary Islands. *Geomorphology*, *416*, 108427. https://doi.org/10.1016/j.geomorph.2022.108427

Rohmer, J., & Dewez, T. (2013). On the deviation of extreme sea-cliff instabilities from the power-law frequency-volume distribution: Practical implications for coastal management. *Journal of Coastal Research*, *165*(65), 1698–1703. https://doi.org/10.2112/SI65-287.1

Romagnoli, C., Casalbore, D., Ricchi, A., Lucchi, F., Quartau, R., Bosman, A., et al. (2018). Morpho-bathymetric and seismo-stratigraphic analysis of the insular shelf of Salina (Aeolian archipelago) to unveil its late-quaternary geological evolution. *Marine Geology*, *395*, 133–151. https://doi.org/10.1016/j.margeo.2017.10.003

Romagnoli, C., & Jakobsson, S. (2015). Post-eruptive morphological evolution of island volcanoes: Surtsey as a modern case study. *Geomorphology*, *250*, 384–396. https://doi.org/10.1016/j.geomorph.2015.09.016

Romagnoli, C., Mancini, F., & Brunelli, R. (2006). Historical shoreline changes at an active island volcano: Stromboli, Italy. *Journal of Coastal Research*, *22*(4), 739–749. https://doi.org/10.2112/05-0554.1

Román, A., Tovar-Sánchez, A., Roque-Atienza, D., Huertas, I. E., Caballero, I., Fraile-Nuez, E., & Navarro, G. (2022). Unmanned aerial vehicles (UAVs) as a tool for hazard assessment: The 2021 eruption of Cumbre Vieja volcano, La Palma Island (Spain). *Science of the Total Environment*, *843*, 157092. https://doi.org/10.1016/j.scitotenv.2022.157092

Roman, J. (2023). Surtsey at 60. *Science*, *382*(6674), 1004. https://doi.org/10.1126/science.adl6569

Romero, J. E., Burton, M., Cáceres, F., Taddeucci, J., Civico, R., Ricci, T., et al. (2022). The initial phase of the 2021 Cumbre Vieja ridge eruption (Canary Islands): Products and dynamics controlling edifice growth and collapse. *Journal of Volcanology and Geothermal Research*, *431*, 107642. https://doi.org/10.1016/j.jvolgeores.2022.107642

Romine, B. M., Fletcher, C. H., Frazer, L. N., Genz, A. S., Barbee, M. M., & Lim, S.-C. (2009). Historical shoreline change, southeast Oahu, Hawaii; applying polynomial models to calculate shoreline change rates. *Journal of Coastal Research*, *25*(6), 1236–1253. https://doi.org/10.2112/08-1070.1

Rosado, B., Fernández-Ros, A., Berrocoso, M., Prates, G., Gárate, J., De Gil, A., & Geyer, A. (2019). Volcano-tectonic dynamics of Deception Island (Antarctica): 27 years of GPS observations (1991–2018). *Journal of Volcanology and Geothermal Research*, *381*, 57–82. https://doi.org/10.1016/j.jvolgeores.2019.05.009

Rosser, N. J., Brain, M. J., Petley, D. N., Lim, M., & Norman, E. C. (2013). Coastline retreat via progressive failure of rocky coastal cliffs. *Geology*, *41*(8), 939–942. https://doi.org/10.1130/G34371.1

Rusu, L., & Rusu, E. (2021). Evaluation of the worldwide wave energy distribution based on ERA5 data and altimeter measurements. *Energies*, *14*(2), 394. https://doi.org/10.3390/en14020394

Sadler, P. M., & Jerolmack, D. J. (2015). Scaling laws for aggradation, denudation and progradation rates: The case for time-scale invariance at sediment sources and sinks. *Geological Society, London, Special Publications*, 69–88. https://doi.org/10.1144/SP404.7

Sayyadi, S., Gudmundsson, M. T., White, J. D., Jónsson, T., Brown, M. C., & Jackson, M. D. (2024). Internal structure of the volcanic island of Surtsey and surroundings: Constraints from a dense aeromagnetic survey. *Journal of Volcanology and Geothermal Research*, *451*, 108096. https://doi.org/10.1016/j.jvolgeores.2024.108096

Scott, W. E., Nye, C. J., Waythomas, C. F., & Neal, C. A. (2010). August 2008 eruption of Kasatochi Volcano, Aleutian Islands, Alaska—Resetting an island landscape. *Arctic Antarctic and Alpine Research*, *42*(3), 250–259. https://doi.org/10.1657/1938-4246-42.3.250

Seabrook, S., Mackay, K., Watson, S. J., Clare, M. A., Hunt, J. E., Yeo, I. A., et al. (2023). Volcaniclastic density currents explain widespread and diverse seafloor impacts of the 2022 Hunga Volcano eruption. *Nature Communications*, *14*(1), 7881. https://doi.org/10.1038/s41467-023-43607-2

Shultz, J. M., Cohen, M. A., Hermosilla, S., Espinel, Z., & McLean, A. (2016). Disaster risk reduction and sustainable development for small island developing states. *Disaster Health*, *3*(1), 32–44. https://doi.org/10.1080/21665044.2016.1173443

Simkin, T., Siebert, L., & Sigurdsson, H. (2000). *Earth's volcanoes and eruptions: An overview* (pp. 249–262). Academic Press.

Smellie, J., López-Martínez, J., Headland, R., Hernández-Cifuentes, F., Maestro, A., Millar, I., et al. (2002). *Geology and geomorphology of Deception Island*. British Antarctic Survey.

Smellie, J., Wilch, T. I., & Rocchi, S. (2013). A 'ā lava-fed deltas: A new reference tool in paleoenvironmental studies. *Geology*, *41*(4), 403–406. https://doi.org/10.1130/G33631.1

Smith, K. J., Baldwin, R., Glatts, R., Chereskin, T. K., Ruhl, H., & Lagun, V. (2003). Weather, ice, and snow conditions at Deception Island, Antarctica: Long time-series photographic monitoring. *Deep Sea Research Part II: Topical Studies in Oceanography*, *50*(10–11), 1649–1664. https://doi.org/10.1016/S0967-0645(03)00084-5

Sofianos, S. S., & Johns, W. E. (2003). An oceanic general circulation model (OGCM) investigation of the Red Sea circulation: 2. Three-dimensional circulation in the Red Sea. *Journal of Geophysical Research*, *108*(C3), 3066. https://doi.org/10.1029/2001JC001185

Sorrentino, L., Cas, R. A., & Stilwell, J. D. (2011). Evolution and facies architecture of Paleogene Surtseyan volcanoes on Chatham Islands, New Zealand, Southwest Pacific Ocean. *Journal of Volcanology and Geothermal Research*, *202*(1–2), 1–21. https://doi.org/10.1016/j.jvolgeores.2010.12.013

Stephenson, W. J., Dickson, M. E., & Denys, P. H. (2017). New insights on the relative contributions of coastal processes and tectonics to shore platform development following the Kaikōura earthquake. *Earth Surface Processes and Landforms*, *42*(13), 2214–2220. https://doi.org/10.1002/esp.4176

Sunamura, T. (1977). A relationship between wave-induced cliff erosion and erosive force of waves. *The Journal of Geology*, *85*(5), 613–618. https://doi.org/10.1086/628209

Sunamura, T. (1992). *Geomorphology of rocky coasts*. Wiley.
Sunamura, T. (1995). Rock control in coastal geomorphic processes. *Transactions - Japanese Geomorphological Union*, *15*(3), 253–272. https://doi.org/10.1016/0148-9062(95)90024-Y
Sunamura, T. (2021). A model for wave abrasion on underwater bedrock, with an application to rapidly downwearing tephra cones adjacent to Surtsey Island in Iceland. *Earth Surface Processes and Landforms*, *46*(8), 1600–1609. https://doi.org/10.1002/esp.5128
Terry, J. P. (2007). *Tropical cyclones: Climatology and impacts in the South Pacific*. Springer Science and Business Media.
Terry, J. P., Goff, J., Winspear, N., Bongolan, V. P., & Fisher, S. (2022). Tonga volcanic eruption and tsunami, January 2022: Globally the most significant opportunity to observe an explosive and tsunamigenic submarine eruption since AD 1883 Krakatau. *Geoscience Letters*, *9*(1), 24. https://doi.org/10.1186/s40562-022-00232-z
Thorarinsson, S. (1969). The last phases of the Surtsey eruption. *Natturufraedingurinn*, *38*, 113–135.
Thorarinsson, S., & Eysteinsson, S. (1967). *Surtsey: The new island in the North Atlantic*. The Viking Press.
Toimil, A., Camus, P., Losada, I., Le Cozannet, G., Nicholls, R., Idier, D., & Maspataud, A. (2020). Climate change-driven coastal erosion modelling in temperate sandy beaches: Methods and uncertainty treatment. *Earth-Science Reviews*, *202*, 103110. https://doi.org/10.1016/j.earscirev.2020.103110
Torrecillas, C., Berrocoso, M., Pérez-López, R., & Torrecillas, M. (2012). Determination of volumetric variations and coastal changes due to historical volcanic eruptions using historical maps and remote-sensing at Deception Island (West-Antarctica). *Geomorphology*, *136*(1), 6–14. https://doi.org/10.1016/j.geomorph.2011.06.017
Torrecillas, C., Zarzuelo, C., de la Fuente, J., Jigena-Antelo, B., & Prates, G. (2024). Evaluation and modelling of the coastal geomorphological changes of deception Island since the 1970 eruption and its involvement in research activity. *Remote Sensing*, *16*(3), 512. https://doi.org/10.3390/rs16030512
Trenhaile, A. S. (2000). Modeling the development of wave-cut shore platforms. *Marine Geology*, *166*(1–4), 163–178. https://doi.org/10.1016/S0025-3227(00)00013-X
Trenhaile, A. S. (2014). Chapter 2 climate change and its impact on rock coasts. *Geological Society, London, Memoirs*, *40*(1), 7–17. https://doi.org/10.1144/M40.2
Trenhaile, A. S. (2015). Coastal notches: Their morphology, formation, and function. *Earth-Science Reviews*, *150*, 285–304. https://doi.org/10.1016/j.earscirev.2015.08.003
Trenhaile, A. S. (2019). Hard-rock coastal modelling: Past practice and future prospects in a changing world. *Journal of Marine Science and Engineering*, *7*(2), 34. https://doi.org/10.3390/jmse7020034
Vaughan, R. G., & Webley, P. W. (2010). Satellite observations of a surtseyan eruption: Hunga Ha'apai, Tonga. *Journal of Volcanology and Geothermal Research*, *198*(1–2), 177–186. https://doi.org/10.1016/j.jvolgeores.2010.08.017
Viggósson, G., & Grétarsson, S. (2010). Landeyjahöfn Ferry Harbour at the South Coast of Iceland. In *Paper presented at PIANC MMX Congress*.
Viðarsdóttir, S. (2019). Hydrodynamic numerical model of waves and currents at Landeyjahöfn Harbour. MSc Thesis.
Walter, T. R., Haghshenas Haghighi, M., Schneider, F. M., Coppola, D., Motagh, M., Saul, J., et al. (2019). Complex hazard cascade culminating in the Anak Krakatau sector collapse. *Nature Communications*, *10*(1), 4339. https://doi.org/10.1038/s41467-019-12284-5
Waythomas, C. F., Scott, W. E., & Nye, C. J. (2010). The geomorphology of an Aleutian volcano following a major eruption: The 7–8 August 2008 eruption of Kasatochi Volcano, Alaska, and its aftermath. *Arctic Antarctic and Alpine Research*, *42*(3), 260–275. https://doi.org/10.1657/1938-4246-42.3.260
Waythomas, C. F., Scott, W. E., Prejean, S. G., Schneider, D. J., Izbekov, P., & Nye, C. J. (2010). The 7–8 August 2008 eruption of Kasatochi Volcano, central Aleutian Islands, Alaska. *Journal of Geophysical Research*, *115*(B12), B00B06. https://doi.org/10.1029/2010JB007437
Wessel, P., Luis, J. F., Uieda, L., Scharroo, R., Wobbe, F., Smith, W. H. F., & Tian, D. (2019). The generic mapping tools version 6 [Software]. *Geochemistry, Geophysics, Geosystems*, *20*(11), 5556–5564. https://doi.org/10.1029/2019GC008515
Wessel, P., & Smith, W. H. (1995). New version of the generic mapping tools. *Eos, Transactions American Geophysical Union*, *76*(33), 329. https://doi.org/10.1029/95EO00198
Whittaker, R. J., & Hanski, I. (1999). *Island biogeography: Ecology, evolution and conservation*. Oxford University Press.387.
Williams, J. G., Rosser, N. J., Hardy, R. J., & Brain, M. J. (2019). The importance of monitoring interval for rockfall magnitude-frequency estimation. *Journal of Geophysical Research: Earth Surface*, *124*(12), 2841–2853. https://doi.org/10.1029/2019JF005225
Williams, R., Rowley, P., & Garthwaite, M. C. (2019). Reconstructing the Anak Krakatau flank collapse that caused the December 2018 Indonesian tsunami. *Geology*, *47*(10), 973–976. https://doi.org/10.1130/G46517.1
Williams, R. S., & Moore, J. G. (1983). *Man against volcano: The eruption on Heimaey, Vestmannaeyjar, Iceland, US department of the interior*. Geological Survey.
Xu, W., Ruch, J., & Jónsson, S. (2015). Birth of two volcanic islands in the southern Red Sea. *Nature Communications*, *6*(1), 7104. https://doi.org/10.1038/ncomms8104
Young, A. P. (2018). Decadal-scale coastal cliff retreat in southern and central California. *Geomorphology*, *300*, 164–175. https://doi.org/10.1016/j.geomorph.2017.10.010
Young, A. P., Guza, R., Flick, R., O'Reilly, W., & Gutierrez, R. (2009). Rain, waves, and short-term evolution of composite seacliffs in southern California. *Marine Geology*, *267*(1–2), 1–7. https://doi.org/10.1016/j.margeo.2009.08.008
Young, A. P., Guza, R., Matsumoto, H., Merrifield, M., O'Reilly, W., & Swirad, Z. (2021). Three years of weekly observations of coastal cliff erosion by waves and rainfall. *Geomorphology*, *375*, 107545. https://doi.org/10.1016/j.geomorph.2020.107545
Zhao, Z., Mitchell, N. C., Quartau, R., Ramalho, R. S., & Rusu, L. (2020). Coastal erosion rates of lava deltas around oceanic islands. *Geomorphology*, *370*, 107410. https://doi.org/10.1016/j.geomorph.2020.107410
Zhao, Z., Mitchell, N. C., Quartau, R., Tempera, F., & Bricheno, L. (2019). Submarine platform development by erosion of a Surtseyan cone at Capelinhos, Faial Island, Azores. *Earth Surface Processes and Landforms*, *44*(15), 2982–3006. https://doi.org/10.1002/esp.4724

References From the Supporting Information

Davies, J. (1964). A morphogenic approach to world shorelines; A morphogenic approach to world shorelines. *Zeitschrift fur Geomorphologie*, *8*(5), 127–142. https://doi.org/10.1127/zfg/mortensen/8/1964/127